Variation of size-segregated particle number concentrations in winter Beijing

Ying Zhou[1], Lubna Dada[1,2]*, Yiliang Liu[3], Yueyun Fu[4], Juha Kangasluoma[1,2], Tommy Chan[1], Chao Yan[2], Biwu Chu[2], Kaspar R Daellenbach[2], Federico Bianchi[2], Tom Kokkonen[2], Yongchun Liu[1], Joni Kujansuu[1,2], Veli-Matti Kerminen[2], Tuukka Petäjä[2], Lin Wang[3], Jingkun Jiang[4], Markku Kulmala[1,2]*

[1]Aerosol and Haze Laboratory, Beijing Advanced Innovation Center for Soft Matter Science and Engineering, Beijing University of Chemical Technology, Beijing, China

[2]Institute for Atmospheric and Earth System Research / Physics, Faculty of Science, University of Helsinki, Finland

[3]Shanghai Key Laboratory of Atmospheric Particle Pollution and Prevention (LAP[3]), Department of Environmental Science & Engineering, Jingwan Campus, Fudan University, Shanghai 200438, China

[4]School of Environment, Tsinghua University, Beijing, China

*Correspondences are to Lubna Dada: lubna.dada@helsinki.fi and Markku Kulmala: markku.kulmala@helsinki.fi

Abstract

The spatial and temporal variability of the number size distribution of aerosol particles is an indicator of the dynamic behavior of Beijing's atmospheric cocktail. This variation reflects the strength of different primary and secondary sources, such as traffic and new particle formation, as well as the main processes affecting the particle population. In this paper, we report size-segregated particle number concentrations observed at a newly-developed Beijing station during the winter of 2018. Our measurements covered particle number size distributions over the diameter range of 1.5 nm-1 μm (cluster mode, nucleation mode, Aitken mode and accumulation mode), thus being descriptive of a major fraction of the processes taking place in the atmosphere of Beijing. Here we focus on explaining the concentration variations in the observed particle modes by relating them to the potential aerosol sources and sinks, and on understanding the connections between these modes. We considered haze days and new particle formation event days separately. Our results show that during the new particle formation (NPF) event days increases in cluster mode particle number concentration were observed, whereas during the haze days high concentrations of accumulation mode particles were present. There was a tight connection between the cluster mode and nucleation mode on both NPF event and haze days. In addition, we correlated the particle number concentrations in different modes with concentrations of trace gases and other parameters measured at

our station. Our results show that the particle number concentration in all the modes correlated with NO$_x$, which reflects the contribution of traffic to the whole sub-micron size range. We also estimated the contribution of ion-induced nucleation in Beijing, and found this contribution to be negligible.

1 Introduction

Atmospheric aerosols are the main ingredient of China's pollution cocktail (Kulmala 2015). Aerosols have gained increasing attention due to their effects on human heath, climate and visibility (Lelieveld et al., 2015, IPCC 2007). Currently, air quality standards for cities in China consider particle mass instead of number concentration (WHO, 2000), which may ignore the potential adverse effect of ultra-fine particles on health (diameter less than 100 nm). It has been shown that ultra-fine particles can penetrate deep into the respiratory tract, ending up to the blood circulation, which allows them to deposit into the brain (Oberdörster et al., 2004). Indeed, studies have pointed out that ultra-fine particles, which contribute to a negligible fraction of the mass concentration, dominate the total number concentration in urban areas (von Bismarck-Osten et al., 2013;Wehner et al., 2004;Wu et al., 2008). Due to their high concentrations, ultrafine particles' toxicological effects are enhanced by their large total surface area (Kreyling et al., 2004).

Apart from their health effects, the temporal and spatial variation of particle number concentrations of different sizes is a good indicator of the strength of their emission sources. Aerosols are emitted either directly as primary particles, such as sea salt or dust particles as a result of natural phenomena (Solomos et al., 2011), or they can be formed through new particle formation (Kulmala, 2003; Kulmala et al., 2004; Kulmala et al., 2013; Kerminen et al., 2018; Chu et al., 2019). Newly formed particles can grow up diameters of 20-100 nm within a day (Kulmala et al., 2004), and they have been found to contribute to a major fraction of the global cloud condensation nuclei population (CCN), thus indirectly affecting the climate (Kerminen et al., 2012). For all aforementioned reasons, and in order to form a collective and complete picture about atmospheric aerosol particles to understand their origin and potential impacts at a specific location, the whole size distribution of these particles needs to be studied.

Recently, due to urbanization and increased population, megacities have increased their contribution to atmospheric aerosol pollution massively (Baklanov et al., 2016). Interestingly, more people live inside eastern Asia (specifically, China and India) than outside this region (https://www.unfpa.org/swop). Therefore, it is important to study the contributions of different sources to size-segregated number concentrations in order to inspire policy makers and the public on measures that need to be taken in order to reduce particulate pollution. Many studies in various cities in China have tackled this topic.

73 For instance, two-years of observations of particle number size distributions at a site in
74 northern Beijing reported that traffic emissions were the major source of nucleation (3-
75 20 nm) and Aitken (20-100 nm) mode particles in urban Beijing (Wang et al., 2013).
76 On the other hand, research conducted in western downtown of Nanjing reported that
77 local new particle formation events were the main contributors of both nucleation (5-
78 20 nm) mode and CCN particle populations (Dai et al., 2017). Measurements of
79 nucleation mode particle concentrations in urban Hong Kong reported the dominant
80 contribution of combustion sources to the nucleation mode (5.5-10 nm) (Wang et al.,
81 2014a), whereas observations in urban Guangzhou found that accumulation and
82 secondary transformation of particles were the main reasons for high concentrations of
83 accumulation mode particles (100-660 nm) (Yue et al., 2010). However, only a few
84 studies in China have reported measurements of cluster mode (sub-3 nm) particles and
85 related them to new particle formation events (Cai et al., 2017;Xiao et al., 2015;Yao et
86 al., 2018;Yu et al., 2016).

87 The observation of sub-3 nm particles and ions has been made possible by recent major
88 developments in instrumentations, such as the particle size magnifier (PSM) (Vanhanen
89 et al., 2011), diethylene glycol-based scanning mobility particle sizer (DEG-SMPS)
90 (Jiang et al., 2011) and Neutral Cluster and Air Ion Spectrometers (NAIS) (Manninen
91 et al., 2016; Mirme et al., 2007).

92 In complicated environments like Beijing, it is very hard to relate each particle mode to
93 a specific source. Indeed, several sources could contribute to aerosol particles in the
94 same size range. For instance, cluster mode particles mainly originate from secondary
95 gas-to-particle transformation processes (Kulmala et al. 2013), although recently also
96 traffic has been identified as a source for these particles (Rönkkö et al., 2017). While
97 cluster mode particles can grow into the Aitken mode , also other sources like traffic
98 contribute to this mode, making the source identification of the Aitken mode
99 complicated (Pirjola et al., 2012). Various anthropogenic activities and biogenic
100 processes contribute to accumulation mode particle sizes. Thus, correlating trace gases
101 and aerosol concentrations of different sizes during different time periods help
102 narrowing down these aerosol sources.

103 In this study, we analyzed the number concentration of four sub-micron aerosol modes:
104 cluster mode (sub-3 nm), nucleation mode (3-25 nm), Aitken mode (25-100 nm), and
105 accumulation mode (100-1000 nm). Our aims were i) to investigate the number
106 concentration variations of size-segregated aerosol number concentrations for each
107 mode, ii) to explore the relationships between the different modes under different
108 atmospheric conditions, iii) to connect the number size distribution modes with multiple
109 trace gases (NO_x, SO_2, CO and O_3) and $PM_{2.5}$ (particulate matter with aerodynamic
110 diameter less than 2.5 μm), and iv) to quantify the contribution of NPF and haze
111 formation to different particle modes in winter time in Beijing. Our work increases
112 understanding on the sources of the different sized particles in Beijing, China, and the

113   work complements studies in other megacities.

114   **2   Materials and Methods**

115   **2.1   Description of SMEAR Beijing station**

116   Beijing, as the capital of China, accommodates more than 20 million people within 16.8
117   thousand square kilometers and only 1.4 thousand square kilometers for urban areas,
118   with an expanding economic activity, construction and industry. Beijing, as one of the
119   largest megacities in the world, is located in the Northern Chinese Plain, and is one of
120   the most industrialized regions in China. Mountains surround Beijing from the west,
121   north and north-west.

122   For our study, we analyzed data collected at the newly-developed station which is part
123   of the Aerosol and Haze Laboratory in Beijing. The urban station follows the concept
124   of Station for Measuring Ecosystem and Atmospheric Relations (SMEAR) (Hari and
125   Kulmala, 2005). Our station is located on the western campus of Beijing University of
126   Chemical Technology (BUCT). It is constructed on the fifth floor of the teaching
127   building on the campus. The sampling lines extend to the rooftop of the building around
128   20 m above the ground level, going directly through windows for selected instruments.
129   The station represents a typical area in urban Beijing subject to pollution sources, such
130   as traffic, cooking and long-range transport of pollution. The campus is surrounded by
131   highways and main roads from the east (3rd ring main road), north (Zizhu road) and
132   south-east (Zizhu Bridge). From the east, west and south, the campus is surrounded by
133   residential and commercial areas.

134   Measurements at SMEAR Beijing started on 16 January, 2018 (Lu et al., 2018). Our
135   measurements continued until present, except during the necessary instruments
136   maintenance and unavoidable factors such as power cuts. The data included in this study
137   were collected between 16 January and 15 March 2018, being representative of Beijing
138   winter conditions.

139   **2.2   Instrumentation**

140   For a comprehensive measurement of particles, a full set of particle measuring
141   instrumentation was operated. First, a nano-condensation nucleus counter system
142   (nCNC) consisting of a Particle Sizer Magnifier (PSM, model A10, Airmodus Oy,
143   Finland) and butanol condensation particle counter (CPC) (model A20, Airmodus Oy,
144   Finland) measured the number concentration of small clusters or particles of 1.2-2.5
145   nm in mobility diameter (Vanhanen et al., 2011). To minimize the sampling losses, the

PSM was sampling horizontally through a window to the north through a short stainless steel sampling inlet extending ~1.2 m outward from the building. The length of the sampling tube was 1.33 m and its inner diameter was 0.8 cm. To further improve the sampling efficiency, a core sampling tube (Kangasluoma et al., 2016) was utilized. The total flow rate was 7.5 liters per minute (lpm), from which 5 lpm was used as a transport flow while the nCNC sample flow rate was 2.5 lpm. In the operation of the PSM, the saturator flow rate scanned from 0.1 to 1.3 lpm and scanned back from 1.3 to 0.1 lpm within 240 s. We averaged the data over 3 scans to make it smoother, and therefore the time resolution of PSM data was 12 minutes. The data were inverted with a kernel function method. When comparing the particle number concentrations obtained with the expectation-maximization method, the cluster mode particle number concentration was, on average, twice higher on the NPF event days and eleven times higher on the haze days (Cai et al., 2018). Therefore, there is some uncertainty in the reported cluster mode particle concentrations.

A particle size distribution (PSD) system measured the particle number size distribution in the size range of 3 nm-10000 nm (Liu et al., 2016). It included a nano-scanning mobility particle sizer (nano SMPS, 3-55 nm, mobility diameter), a long SMPS (25-650 nm, mobility diameter) and an aerodynamic particle sizer (APS, 0.55 μm-10 μm, aerodynamic diameter). The PSD system sampled from the rooftop using a 3-m-long sampling tube. A cyclone that removed particles larger than 10 μm was added in front of the sample line. The time resolution of PSD system data was 5 minutes.

A Neutral Cluster and Air Ion Spectrometer (NAIS, model 4-11, Airel, Estonia) measured number size distributions of particles (2.5-42 nm, mobility diameter) and ions (0.7-42 nm, mobility diameter) (Manninen et al., 2016; Mirme and Mirme, 2013). It switched between detecting either naturally charged ions or total particles (including the uncharged fraction) with unipolar charging. It measured 2 min in the neutral mode, 2 min in the ion mode and then offset for 30 seconds for every measurement cycle. The NAIS was sampling horizontally from the north window. The copper sampling tube with an outer diameter of 4 cm extended 1.6 m outside the window. To increase the sampling efficiency, the sampling flow rate was 54 lpm.

The trace gas monitors measured carbon monoxide (CO), sulfur dioxide (SO_2), nitrogen oxides (NO_x) and ozone (O_3) concentrations with Thermo Environmental Instruments models 48i, 43i-TLE, 42i, 49i, respectively. They all sampled through a common inlet through the roof of the building. The length of the sampling tube was approximately 3 m. The time resolution of CO, NO_x, and O_3 data were 5 minutes, whereas the time resolution of SO_2 data was 1 hour before 22 January, 2018, and 5 minutes after that.

The $PM_{2.5}$ data were obtained from the nearest national monitor station, Wanliu station, around 3 km north of our station. The $PM_{2.5}$ data from Wanliu station compared nicely with the $PM_{2.5}$ data from three other adjacent national stations. The time resolution of

185 the PM$_{2.5}$ data was 1 hour, and these data were recorded every hour. Detailed
186 information is reported in Cao et al. (2014).

187 We measured the relative humidity (RH, %), visibility (km), wind speed (m/s) and wind
188 direction (˚) from a weather station on the roof of our station.

189 When data sets having different time resolutions were used, we chose the smallest time
190 resolution as the common time resolution. Data with higher time resolutions were
191 merged to the common time resolution by taking median numbers between two time
192 points of the new time series.

2.3 NPF events and haze days classification

194 We classified days into "NPF event days" and "haze days". The days that did not fit
195 either of these two categories were marked as "Other days", and they were excluded
196 from our future analysis unless otherwise specified. We observed 28 NPF event days
197 and 24 haze days in total. Table 1 describes the specific calendar of events with the
198 aforementioned categories of days.

199 We identified the NPF event days following the method introduced in (Dal Maso et al.,
200 2005), which requires an appearance of a new mode below 25 nm and that the new
201 mode shows signs of growth for several hours (Dal Maso et al., 2005; Kulmala et al.,
202 2012). Haze events were identified as having a visibility less than 10 km and ambient
203 relative humidity below 80% (China Meteorological Administration). Individual days
204 were classified as haze days when the haze event lasted for at least 12 consecutive hours.
205 During our study periods, there was no overlap between the NPF events and haze days,
206 as these two phenomena never occurred simultaneously. While the NPF events
207 appeared right after sunrise and lasted for several hours, the haze events did not have
208 any specific time of appearance but lasted from a few hours up to several days.

209 The particle number size distribution was divided into 4 modes according to their
210 diameter: cluster mode (sub-3 nm), nucleation mode (3-25 nm), Aitken mode (25-100
211 nm), and accumulation mode (100-1000 nm). We calculated cluster mode particle
212 number concentrations using Particle Size Magnifier (PSM) data, nucleation mode
213 particle number concentration using Neutral Cluster and Air Ion Spectrometer (NAIS)
214 particle mode data, and Aitken and accumulation mode particle number concentrations
215 using Particle Size Distribution (PSD) system data. The Particle Size Distribution
216 system (PSD) and Neutral Cluster and Air Ion Spectrometer (NAIS) had an overlapping
217 particle size distribution over the mobility diameter range of 3-42 nm. As shown in
218 Figure S1, total particle number concentrations from the NAIS and PSD system
219 correlated well with each other on both NPF event days (R^2 was 0.92) and haze days
220 (R^2 was 0.90) in the overlapping size range. The slopes between the total particle
221 number concentration from the PSD system and that from the NAIS were 0.90 and 0.85

222 on the NPF event days and haze days, respectively. The particle number size
223 distribution in the overlapping size range of the NAIS and PSD system matched well
224 on both NPF event days and haze days as shown in Figure S2.

225 Moreover, since new particle formation events were only observed during daytime in
226 Beijing, our analysis concentrated mostly on the time period 8:00 to 14:00, unless
227 specified otherwise.

228 **2.4   Parameter calculation**

229 *2.4.1 Calculation of the growth rate*

230 The growth rates of cluster and nucleation mode particles were calculated from positive
231 ion data and particle data from Neutral Cluster and Air Ion Spectrometer (NAIS),
232 respectively, by using the appearance time method introduced by Lehtipalo et al. (2014).
233 In this method, the particle number concentration of particles of size dp is recorded as
234 a function of time, and the appearance time of particles of size dp is determined as the
235 time when their number concentration reaches 50% of its maximum value during new
236 particle formation (NPF) events.

237 The growth rates (GR) were calculated according to:

238
$$GR = \frac{dp_2 - dp_1}{t_2 - t_1} \tag{1}$$

239 where t_2 and t_1 are the appearance times of particles with sizes of dp_2 and dp_1
240 respectively. Figure S3 shows an example of how this method was used.

241 *2.4.2 Calculation of the coagulation sink*

242 The coagulation sink (CoagS) was calculated according to the equation (2) introduced
243 by Kulmala et al. (2012):

244

245
$$CoagS_{dp} = \int K(dp, d'p) n(d'p) \, dd'p \cong \sum_{d'p=dp}^{d'p=max} K(dp, d'p) N_{d'p}$$

246
$$\tag{2}$$

247 where $K(dp, d'p)$ is the coagulation coefficient of particles with sizes of dp and
248 $d'p$, $N_{d'p}$ is the particle number concentration with size of $d'p$.

2.4.3 Calculation of the formation rate

The formation rate of 1.5-nm particles ($J_{1.5}$) was calculated using particle number concentrations measured with a Particle Sizer Magnifier (PSM). The formation rate of 1.5-nm ions ($J_{1.5}^{\pm}$) was calculated using positive and negative ions data from the Neutral Cluster and Air Ion Spectrometer (NAIS) as well as PSM data. The upper limit used was 3 nm. The values of $J_{1.5}$ and $J_{1.5}^{\pm}$ were calculated following the methods introduced by Kulmala et al. (2012) with equation (3) and equation (4), respectively:

$$J_{dp} = \frac{dN_{dp}}{dt} + CoagS_{dp} \cdot N_{dp} + \frac{GR}{\Delta dp} \cdot N_{dp} \qquad (3)$$

where $CoagS_{dp}$ is the coagulation sink in the size range of $[dp, dp + \Delta dp]$ and GR is the growth rate.

$$J_{dp}^{\pm} = \frac{dN_{dp}^{\pm}}{dt} + CoagS_{dp} \cdot N_{dp}^{\pm} + \frac{GR}{\Delta dp} \cdot N_{dp}^{\pm} + \alpha \cdot N_{dp}^{\pm} \cdot N_{<dp}^{\mp} - \chi N_{dp} \cdot N_{<dp}^{\pm} \qquad (4)$$

The fourth and fifth terms on the right hand side of equation (4) represent ion-ion recombination and charging of neutral particles by smaller ions, respectively, α is the ion-ion recombination coefficient and χ is the ion-aerosol attachment coefficient.

3   Results and discussion

3.1 General character of particle modes and trace gases

3.1.1 Sub-micron particles and PM2.5

Particle number concentrations of different modes varied depending on the period, as shown in Figure 1. We observed that the cluster and nucleation mode particle concentrations were the highest on the NPF event days. In fact, the cluster and nucleation mode particles dominated the total particle number concentration with an average contribution of 96% (Figure 2). On the haze days, the average contribution levels of the four modes were about equal. Aitken and accumulation mode particles contributed to 52% of the total particle number concentration on the haze days, as compared to 4% on the NPF event days.

On the haze days, we observed a surprising concentration of cluster mode particles in spite of the high concentrations of Aitken and accumulation particles. Since large particles are expected to efficiently scavenge clusters and smallest growing particles by coagulation (Kerminen et al., 2001; Kulmala et al., 2017), this is indicative of either airborne cluster formation (Kulmala et al., 2007) or vehicular emissions of clusters and nucleation mode particles (e.g. Rönkkö et al., 2017) during haze. The ratio between

nucleation mode and cluster mode particle median number concentration was close to unity (0.84), which might indicate their common source on haze days, in comparison to the smaller ratio of 0.3 during the NPF days. It is therefore likely that the primary particles dominated the nucleation mode on the haze days, while the growth of cluster mode particles into nucleation mode explains the nucleation mode particles on NPF days.

The median concentrations of Aitken and accumulation mode particles were 16000 cm^{-3} and 17500 cm^{-3}, respectively, on the haze days and 8240 cm^{-3} and 1670 cm^{-3}, respectively, on the NPF event days. Overall, these concentrations were a factor of 2.1 and 10.5 times higher on the haze days than on the NPF event days. The PM$_{2.5}$ mass concentration was clearly higher on the haze days compared with the NPF event days (Figure 3). The PM$_{2.5}$ mass concentration in urban areas is dominated by accumulation mode particles, with a clearly smaller a contribution by ultrafine (cluster, nucleation and Aitken mode) particles (Feng et al., 2010).

3.1.2 Trace gases

In this work, we considered four trace gases (SO$_2$, CO, NO$_x$ and O$_3$) in our analysis (Figure 4), as these compounds are most commonly used to evaluate air quality and pollution sources in China (Hao and Wang, 2005; Han et al., 2011). During our observation period, the median concentrations of SO$_2$, CO, NO$_x$ on haze days were 5.1, 1400 and 27 ppb, respectively. While high, these concentrations are lower than the corresponding concentrations (18, 2200, 75 ppb, respectively) during the extremely severe haze episode that took place in Beijing in January 2013 (Wang et al., 2014b). The median concentration of O$_3$ was 10 ppb on the haze days during our observations, a little bit higher than the severe haze episode in 2013 (<7 ppb; Wang et al., 2014b).

The median levels of SO$_2$, CO, NO$_x$ and O$_3$ were 230%, 50%, 100% and 50% higher, respectively, on the haze days than on the NPF days. SO$_2$, CO and NO$_x$ are usually considered tracers of primary pollution, so their lower levels on the NPF event days indicates that relatively clean conditions favor NPF events (Vahlsing and Smith, 2012;Tian et al., 2018).

3.2 Diurnal behavior

In order to draw a clear picture of the evolution of size-segregated particle number concentrations, we analyzed the diurnal concentration behavior of the different trace gases (Figure 5) and particle modes (Figure 6).

Since trace gases have more definitive sources than particles, we can get some insight into particle sources by comparing their diurnal patterns with those of particles in different modes. For instance, CO is usually emitted as the by-product of inefficient

316 combustion of biomass or fossil fuels (Pétron et al., 2004; Lowry et al., 2016). We
317 observed similar diurnal patterns for NO_x and CO, with an increase during the morning
318 rush hours followed by another peak at around 15:00, suggesting similar sources. Due
319 to lower human activities and traffic during nighttime, lower concentrations of NO_x and
320 CO were observed. Earlier observations in urban areas having high NO_x concentrations
321 found that O_3 was consumed by its reaction with NO, while NO_2 works as precursor
322 for O_3 via photochemical reactions (Wang et al., 2017). In our observations, the diurnal
323 pattern of O_3 was opposite to that of NO_x, which is consistent with O_3 loss by large
324 amounts of freshly emitted NO during rush hours and O_3 production by photochemical
325 reactions involving NO_2 after the rush hours in the morning.

326 In Figure 7, we show the median diurnal pattern of particle number size distribution on
327 the NPF event days and haze days separately. On the NPF event days, we observed
328 cluster formation from diameters smaller than 3 nm. The growth of newly-formed
329 particles lasted for several hours, resulting in a consecutive increase of the particle
330 number concentrations in all the four modes. During traffic rush hours in the morning
331 and evening, we observed an increase of particle number concentrations in the size
332 range of cluster mode to around 100 nm.

333 On the haze days, we still observed an increase of particle number concentration in the
334 size range of cluster mode to Aitken mode during rush hours. Traditionally, NPF events
335 occur during the time window between sunrise and sunset by photochemical reactions
336 (Kerminen et al., 2018). The binary or ternary nucleation between sulfuric acid and
337 water, ammonia or amines are usually thought of as sources of atmospheric cluster
338 mode particles, especially in heavily polluted environments (Kulmala et al., 2013;
339 Kulmala et al., 2014; Yao et al., 2018; Chu et al., 2019). The burst of cluster mode
340 particle number concentration outside the traditional NPF time window, especially
341 during the rush hours in the afternoon, suggests a very different source of cluster mode
342 particles from traditional nucleation, e.g. nucleation from gases emitted by traffic
343 (Rönkkö et al., 2017).

344 As shown in Figure 6, on the NPF event days, the cluster mode particle number
345 concentration started to increase at the time of sunrise and peaked around noon with a
346 wide single peak, showing the typical behavior related to NPF events (Kulmala et al.,
347 2012). Comparatively, on the haze days, the cluster mode particle number concentration
348 showed a double peak pattern similar to the diurnal cycle of NO_x (Figure 5). This
349 observation in consistent with our discussion above that traffic emission possibly
350 contributed to cluster mode particles. By comparing cluster mode particle number
351 concentrations between the haze days and NPF event days, we estimated that traffic-
352 related cluster mode particles could contribute up to 40-50 % of the total cluster mode
353 particle number concentration on the NPF event days.

354 Similar to the cluster mode, the nucleation mode had a single peak on the NPF event

days. Nucleation mode particle number concentrations started to increase shortly after the corresponding increases in the cluster mode, which could be attributed to the growth of cluster mode particles into the nucleation mode. The observed peak of the nucleation mode particle number concentrations had a shoulder at around 7:00 - 9:00 concurrent with the morning peak of the NO_x concentration, which indicates a contribution from traffic to the nucleation mode. It is important to note, however, that the height of this shoulder was only 20% of the maximum nucleation mode particle number concentration. These results suggest that, compared with atmospheric NPF, traffic contributed much less to the nucleation mode particle number concentration.

During the haze days, the diurnal pattern of the nucleation mode particle number concentration reminded that of NO_x, showing no peak during the daytime between the rush hours. This suggests that the nucleation mode particles were dominantly from traffic emissions on the haze days. Additionally, it is important to note that during the haze days, we observed different maximum concentrations for morning versus evening peaks, implying a higher contribution of traffic in the morning than in the afternoon. This result is in line with the diurnal cycle of NO_x during the haze days.

On the NPF even days, Aitken mode particles are mainly attributed to two different sources hard to be distinguished from each other: primary and secondary sources, such as combustion and growth of newly formed particles, respectively. In comparison to the cluster and nucleation modes that had pronounced diurnal cycles during the NPF event days, the Aitken mode particle number concentration had a pattern similar to NO_x before 9:00 in the morning. This implies that traffic emissions were important sources to maintain Aitken mode particle concentrations in the morning hours. The Aitken mode particle number concentration increased during the afternoon hours, probably due to the growth of the nucleation mode particles via multicomponent condensation and possibly some other gas-to-particle conversion pathways. The concurrent decrease of the nucleation mode particle number concentration supports this view. The Aitken mode particle number concentration increase in the evening was concurrent with the increase of CO and NO_x, which could be attributed to combustion sources (Roberts and Jones, 2004; Koponen et al., 2001).

On the haze days, the Aitken mode particle number concentration experienced little change before about 14:00, contrary to both CO and NO_x concentrations, indicating a small contribution by primary sources during that time of the day. It is important to mention that the growth of particles is not limited to the days when new particle formation occurs. In fact, on the haze days, the wind was typically more stagnant, reducing the vertical mixing of pollutants and their horizontal advection (Zheng et al., 2015). The increase of Aitken mode particle number concentration started at around 16:00 and peaked at around 20:00 similar to the NPF event days. This is concurrent with the increase in the NO_x and CO concentrations, which might be attributed to traffic emissions.

395 The concentration of accumulation mode particles was an order of magnitude higher
396 during the haze days compared with the NPF days, causing a higher condensation sink
397 (on average 0.015 s^{-1} for the NPF event days and 0.10 s^{-1} for the haze days, as shown
398 in Figure S4), and thus introducing a reason why NPF did not take place on the haze
399 days (Kulmala et al., 2017). The concentration, on the other hand, did not experience
400 much diurnal variation. There was a slight increase in the accumulation mode particle
401 number concentration during the morning rush hours starting at around 6:00 concurrent
402 with the increase in the Aitken mode particle number concentration. The second slight
403 increase started at around 16:00, two hours later than that of the Aitken mode,
404 suggesting a secondary contribution to accumulation mode particles. On the NPF event
405 days, the accumulation mode had the similar diurnal pattern as SO_2, implying that SO_2
406 participated in the formation of accumulation mode on the NPF event days.

407 **3.3 Correlation between the particle modes and trace gas and PM$_{2.5}$ concentrations**

408 Beijing's atmosphere is a very complicated environment (Kulmala, 2015). Aerosol
409 particles in the atmosphere of Beijing are subject to aerosol dynamical processes,
410 surface reactions, coagulation, deposition and transport, thus hindering direct
411 connection with their sources based on physical size distributions only. However, by
412 correlating each particle mode to various trace gases, we can get indications on the
413 sources of particles. In this section, we use CO, SO_2, NO_x and O_3 as tracers. By
414 examining responses of size-segregated particle number concentrations to changes in
415 trace gas and PM$_{2.5}$ concentrations (Table 2a and Table 2b), we can get further insights
416 into the main sources of particles in each mode and into the dynamical processes
417 experienced by these particles under different pollution levels. Of course, not all
418 sources or dynamics can be captured using this approach. In addition, due to the
419 complex physical and chemical processes experienced by the particles, the correlation
420 analysis cannot quantify the strength of individual sources or dynamical processes.

421 *3.3.1 Connection with SO$_2$*

422 SO_2 is a key precursor for H_2SO_4 through photochemical reactions in Beijing, which is
423 in turn a requirement for new particle formation in megacity environments (Wang et al.,
424 2013; Yao et al., 2018). Although being a very important precursor of NPF, SO_2 had
425 lower concentrations   on the NPF event days than on the haze days (Figure 8). High
426 concentrations of SO_2 have been ascribed to regional pollution and anthropogenic
427 condensation sink even in semi-pristine environments (Dada et al., 2017). Earlier
428 observations report that the main sources of SO_2 are power plants, traffic and industry,
429 so SO_2 can be used as a tracer for regional pollution (Yang et al., 2018;Lu et al., 2010).

430 Generally, as shown in Figure 8, the SO_2 concentration correlated negatively with both

cluster and nucleation mode particle number concentrations. Higher SO_2 concentrations were encountered on more polluted days when NPF events were suppressed due to the high particle loadings, explaining the overall negative correlation. However, if we look at the NPF event days and haze days separately, we cannot see any clear correlation between the SO_2 concentration and cluster mode or nucleation mode particle number concentration, as shown also in Table 2a and Table 2b. This result indicates that during our observations, NPF occurred in relatively clean conditions, but the strength of a NPF event was not sensitive to the regional pollution level as long as NPF was able to occur.

On the NPF event days, the SO_2 concentration correlated positively with the concentrations of both Aitken and accumulation mode particles during the chosen NPF time window, whereas on the haze days no correlation between the SO_2 concentration and Aitken mode particle number concentration could be observed. This suggests that regional and transported pollution contributed to Aitken and accumulation mode particles on the NPF event days, while on haze days the transported and regional pollution was only a prominent factor affecting accumulation mode particle number concentration. In addition, SO_2 contributes to heterogeneous reactions on particle surfaces, explaining that a fraction of accumulation mode particles could have resulted from the growth of Aitken mode particles (Ravishankara., 1997).

3.3.2 Connection with NOx

NO_x is usually considered as the pollution tracer mainly from traffic (Beevers et al., 2012). As shown in Table 2a and Figure 9, the NO_x concentration correlated negatively with both cluster and nucleation mode particle number concentrations on the NPF event days. Compared with the correlation between SO_2 and cluster and nucleation mode particle number concentrations, this result indicates that local traffic emissions affected cluster and nucleation mode particles more than regional pollution on the NPF event days.

On the haze days, we did not see any correlation between the cluster mode particle number concentration and NO_x concentration (Table 2b), although according to our analysis above, traffic emissions can be the source of cluster mode particles during the haze days. One possible reason for this is that the relationship between cluster mode particle number concentration and NO_x concentration was not linear. Earlier studies pointed out that the dilution ratio is the dominant factor affecting the number size distribution of nanoparticles generated from traffic gases emissions (Shi and Harrison, 1999; Shi et al., 2001). Temperature and humidity were also identified as factors affecting nanoparticle number size distribution nucleated from tailpipe emissions (Shi et al., 2001). Such factors would decrease the correlation between the cluster and nucleation mode particle number concentrations and NO_x concentration.

The Aitken mode particle number concentration correlated positively with the NO_x concentration on both NPF event days and haze days, suggesting that traffic emissions

470 might be an important source of Aitken mode particles.

471 The accumulation mode particle number concentration correlated positively with the
472 NO_x concentration on the NPF event days, which is consistent with earlier studies
473 showing that traffic emissions can contribute to accumulation mode particles in urban
474 areas (Vu et al., 2015). On the haze days, the accumulation mode particle number
475 concentration correlated less with NO_x than with SO_2, suggesting that regional and
476 transported pollution was a more important contributor to accumulation mode particles
477 than traffic emissions.

3.3.3 Connection with CO

479 CO has some similar sources as NO_x, such as traffic. On the NPF event days, the CO
480 concentration correlated with particle number concentrations in each mode in a very
481 similar way as NO_x did, suggesting that CO and NO_x had common sources, such as
482 traffic emissions, on the NPF event days. This result confirms our analysis above that
483 traffic emissions could suppress NPF and growth on the NPF event days, in addition to
484 which they might be important sources of the Aitken and accumulation mode particles.

485 On the haze days, CO transported from polluted areas dominated the total CO
486 concentration. The CO concentration had a positive correlation with the accumulation
487 mode particle number concentration, but no clear correlation with the particle number
488 concentration of the three other modes. This result confirms our analysis above that on
489 the haze days, local emissions dominated Aitken particle number concentrations while
490 regional and transported pollutions affected accumulation mode particle number
491 concentrations more than local emissions.

3.3.4 Connection with O_3

493 Ozone is a secondary pollution trace gas and its concentration represents the oxidization
494 capacity of atmosphere. Earlier observations found that high O_3 concentrations favor
495 NPF by enhancing photochemical reactions (Qi et al., 2015). However, we did not see
496 any correlation between the O_3 concentration and cluster mode particle number
497 concentration, suggesting that O_3 was not the limiting factor for cluster mode particle
498 number concentration.

499 The O_3 concentration correlated positively with both nucleation and Aitken mode
500 particle number concentration on the NPF event days during the NPF time window,
501 whereas on the haze days O_3 concentration correlated only with the Aitken mode
502 particle number concentration.

503 The above results suggest that O_3 influences heterogeneous reactions and particle
504 growth rather than the formation of new aerosol particles.

3.3.5 Connection to PM2.5

As shown in Figure 10, the $PM_{2.5}$ concentration correlated negatively with the cluster and nucleation mode particle number concentrations, and positively with the accumulation mode particle number concentration. High $PM_{2.5}$ concentrations tend to suppress NPF by increasing the sinks of vapors responsible for nucleation and growth of cluster and nucleation mode particles. The particles causing high $PM_{2.5}$ concentrations also serve as sinks of cluster and nucleation mode particles by coagulation.

As shown in Table 2a and Figure 12, the Aitken mode particle number concentration correlated positively with the $PM_{2.5}$ concentration on the NPF event days. A possible reason for this could be the tight connection between the Aitken and accumulation mode particles on the NPF event days (Table 3a), and the observation that accumulation mode particles are usually the main contributor to $PM_{2.5}$ in Beijing (Liu et al., 2013). On the haze days, the Aitken mode particle number concentration correlated negatively with the $PM_{2.5}$ concentration (Table 2b). A possible reason for this is that pre-existing large particles acted as a sink for Aitken mode particles by coagulation as well as a sink for vapors responsible for the growth of smaller particles into the Aitken mode. In addition, while $PM_{2.5}$ is dominated by regional and transported secondary aerosols, Aitken mode particles mainly originate from local emissions such as traffic and cooking in Beijing (Wu et al., 2007; Wang et al., 2013; Du et al., 2017; de Jesus et al., 2019).

3.4 Correlation between different particle modes

Table 3a and Table 3b as well as Figure 11 show the correlation between particle number concentrations in different modes. On the NPF event days, cluster and nucleation mode particle number concentrations correlated positively with each other due to their common dominant source, NPF. Both cluster and nucleation mode particle number concentrations correlated negatively with the Aitken and accumulation mode particle number concentrations because, as discussed earlier, high concentrations of large particles tend to suppress NPF and subsequent growth of newly-formed particles.

On the NPF event days, Aitken and accumulation mode particle number concentrations correlated positively with each other, as well as with the SO_2 and NO_x concentration. This suggests that on the NPF event days, Aitken and accumulation mode particles both formed during regional transportation as secondary particles and were emitted by traffic as primary particles.

On the haze days, cluster and nucleation mode particle number concentrations correlated positively with each other, and with the Aitken mode particle number concentration. This is suggestive of a similar dominating sources for these particle,

541 most likely traffic emissions. Similar to the NPF event days, cluster and nucleation
542 mode particle number concentrations correlated negatively with the accumulation mode
543 particle number concentration, even though this correlation was rather weak (Table 3b).
544 As expected based on the discussion in section 3.3.5, the Aitken mode particle number
545 concentration had a negative correlation with the accumulation mode particle number
546 concentration on the haze days.

547 **3.5 Atmospheric ions and ion induced nucleation in Beijing**

548 In order to estimate the contribution of ions to the total cluster mode particle number
549 concentration and the importance of ion induced nucleation in Beijing, we studied ion
550 number concentrations in the size range of 0.8-7 nm by dividing them into 3 sub-size
551 bins: constant pool (0.8-1.5 nm), charged clusters (1.5-3 nm) and larger ions (3-7 nm).
552 As shown in Figure 12, number concentrations of positive ions were higher than those
553 negative ions in all the size bins on both NPF event days and haze days. We will only
554 discuss positive ions here.

555 The median number concentration of positive ions in the constant pool on NPF event
556 days was only 100 cm^{-3} in Beijing, much less than that in the boreal forest (600 cm^{-3};
557 Mazon et al., 2016). Also, the median number concentration of positive charged clusters
558 was 20 cm^{-3} on the NPF event days, and the ratio to the total cluster mode particle
559 number concentration was 0.001 to 0.004 during the NPF time window (Figure 13).
560 This ratio is comparable to that observed in San Pietro Capofiume (0.004), in which the
561 anthropogenic pollution level was also high, but clearly lower than that observed in
562 another megacity in China, Nanjing (0.02; Kontkanen et al., 2017). Considerably higher
563 ratios were observed in clean environments, for example during winter in the boreal
564 forest at Hyytiälä, Finland (0.7; Kontkanen et al., 2017). The median number
565 concentration of larger ions (3-7 nm) on the NPF event days was 30 cm^{-3}, a little bit
566 higher than the charged cluster mode particle number concentration, indicating that not
567 all of the larger ions originate from the growth of charged clusters, but rather from
568 charging of neutral particles by smaller ions. On the haze days, charged ion number
569 concentrations were much lower than those on the NPF days, which could be attributed
570 to the higher condensation sink.

571 The diurnal pattern of the ratio of number concentration between charged and total
572 cluster mode particles was the highest during the night with a maximum of 0.008, and
573 had a trough during daytime with a minimum of 0.001 on the NPF event days. Such
574 diurnal pattern is similar to earlier observations in Nanjing, San Pietro Capofiume and
575 Hyytiälä (Kontkanen et al., 2017). This ratio reached its minimum around noon,
576 because the total cluster mode particle number concentration reached its maximum
577 around that time due to NPF. The ratio had a small peak at around 9:00, similar to earlier
578 observations in Centreville and Po Valley (Kontkanen et al., 2016;Kontkanen et al.,

2017). The possible reason is that charged clusters were activated earlier in the morning than neutral clusters. The ratio increased from the midnight until about 4:00, similar to the number concentration of charged clusters.

As shown in Figure 14, the diurnal median of the ratio between the formation rate of positive ions of 1.5 nm ($J_{1.5}^{+}$) and the total formation rate clusters of 1.5 nm ($J_{1.5}$) varied from 0.0009 to 0.006. This result is comparable to observations in Shanghai, where the positive ion induced nucleation contributed only 0.05% to the total formation rate of 1.7-nm particles ($J_{1.7}$) (Yao et al., 2018).

3.6 Particle growth rates

The growth rates of particles generated from NPF events were examined in three size ranges: <3 nm, 3-7 nm and 7- 25 nm (Figure 15). The median growth rates of particles in these size ranges were 1.0 nm/h, 2.7 nm/h and 5.5 nm/h, respectively. The growth rate of cluster mode particles was comparable with that observed in Shanghai (1.5 nm/h; Yao et al., 2018). The notable increase of the particle growth rate with an increasing particle size is a very typical feature in the sub-20 nm size range (Kerminen et al., 2018), and it may also extend to larger particle sizes (Paasonen et al., 2018).

Our observations are in line with the reported range of nucleation mode particle growth rates of 0.1-11.2 nm/h in urban areas of Beijing (Wang et al., 2017b; Jayaratne et al., 2017). Such growth rates can explain the observed increases of Aitken mode particle number concentrations in the afternoon.

4   Summary and conclusions

We measured particle number concentrations over a wide range of particle diameters (1.5-1000 nm) on both NPF event days and haze days in winter Beijing. To our knowledge, this was the first time when cluster mode particle number concentrations have been reported on haze days in Beijing.

The observed responses of particle number concentrations in different modes (cluster, nucleation, Aitken and accumulation mode) to changes in trace gas and $PM_{2.5}$ concentrations were quite heterogeneous, suggesting different sources and dynamics experienced by each mode. NPF was the dominant source of cluster and nucleation mode particles. Ion-induced nucleation did not play an important role during the NPF events. The growth rates of cluster and nucleation mode particles increased with an increasing particle size. Traffic emissions contributed to every mode and were the dominant source of cluster and nucleation mode particles on the haze days. The main sources of Aitken mode particles were local emissions, while transported and regional

pollution as well as growth from the nucleation mode also contributed to the Aitken mode. The main source of accumulation mode particles was regional and transported pollution. $PM_{2.5}$ affected the number concentration of sub-100 nm particles by competing for vapors responsible for particle growth and by acting as sinks for particles by coagulation. The main contributors to the $PM_{2.5}$ mass concentration were accumulation mode particles on the haze days.

As demonstrated here and in many other studies (e.g. Brines et al., 2015), ultrafine particles (< 100 nm in diameter) tend to dominate the total aerosol particle number concentration in megacities like Beijing. More attention should therefore put on ultrafine particles in urban environments. We found that both NPF and traffic emissions are important sources of ultrafine particles in Beijing. To improve our understanding on the potential effects of ultrafine particles on health and air quality, we need to do more research on their sources and physical and chemical properties. Laboratory and model analysis on dynamics of ultrafine particles would help us to understand the evolution of particle number size distributions. In addition, to identify and locate other possible sources, long-term observations on ultrafine particles down to the cluster mode as well as source apportionment analyses, such as cluster analysis and receptor model studies, are still needed. Ultrafine particles should also be taken into consideration when making policies to control air pollution. New regulations should be designed to control primary emission sources, such as traffic, or precursor emissions for secondary ultrafine particles involving NPF and subsequent particle growth.

5 Acknowledgments

Author contributions. YZ, YiL, YF, JuK contributed to data collection. YZ, TC, LD contributed to data inversion. YZ and LD contributed to analyzing the data. CY, BC, KRD, FB, TK, YoL, JoK contributed to maintaining the station. YZ, LD, JuK, VMK wrote the paper. TP, LW, JJ, MK provided helpful scientific discussions. All co-authors reviewed the manuscript.

Competing interests. The authors declare that they have no conflict of interest.

651

6   References

652

653   Baklanov, A., Molina, L. T., and Gauss, M.: Megacities, air quality and climate,
654   Atmospheric Environment, 126, 235-249,
655   https://doi.org/10.1016/j.atmosenv.2015.11.059, 2016.

656   Beevers, S. D., Westmoreland, E., de Jong, M. C., Williams, M. L., and Carslaw, D. C.:
657   Trends in NOx and NO2 emissions from road traffic in Great Britain,
658   Atmospheric Environment, 54, 107-116,
659   https://doi.org/10.1016/j.atmosenv.2012.02.028, 2012.

660   Brines, M., Dall'Osto, M., Beddows, D. C. S., Harrison, R. M., Gomez-Moreno, F.,
661   Nunez, L., Artinano, B., Costabile, F., Gobbi, G. P., Salimi, F., Morawska, L.,
662   Sioutas, C., and Querol, X.: Traffic and nucleation events as main sources of
663   ultrafine particles in high-insolation developed world cities, Atmos Chem Phys,
664   15, 5929-5945, 2015.

665   Cai, R. L., Yang, D. S., Fu, Y. Y., Wang, X., Li, X. X., Ma, Y., Hao, J. M., Zheng, J.,
666   and Jiang, J. K.: Aerosol surface area concentration: a governing factor in new
667   particle formation in Beijing, Atmos Chem Phys, 17, 12327-12340,
668   https://doi.org/10.5194/acp-2017-467, 2017.

669   Cai, R. L., Yang, D. S., Ahonen, L. R., Shi, L. L., Korhonen, F., Ma, Y., Hao, J. M.,
670   Petaja, T., Zheng, J., Kangasluoma, J., and Jiang, J. K.: Data inversion methods
671   to determine sub-3 nm aerosol size distributions using the particle size magnifier,
672   Atmos Meas Tech, 11, 4477-4491, 2018.

673   Cao, C., Jiang, W. J., Wang, B. Y., Fang, J. H., Lang, J. D., Tian, G., Jiang, J. K., and
674   Zhu, T. F.: Inhalable Microorganisms in Beijing's PM2.5 and PM10 Pollutants
675   during a Severe Smog Event, Environ Sci Technol, 48, 1499-1507,
676   https://doi.org/10.1021/es4048472, 2014.

677   Chu, B. W., Kerminen, V. M., Bianchi, F., Yan, C., Petäjä, T., and Kulmala, M.:
678   Atmospheric new particle formation in China, Atmos Chem Phys, 19, 115-138,
679   https://doi.org/10.5194/acp-19-115-2019, 2019.

680   Dada, L., Paasonen, P., Nieminen, T., Mazon, S. B., Kontkanen, J., Peräkylä, O.,
681   Lehtipalo, K., Hussein, T., Petäjä, T., Kerminen, V. M., Bäck, J., and Kulmala,
682   M.: Long-term analysis of clear-sky new particle formation events and nonevents
683   in Hyytiälä, Atmos Chem Phys, 17, 6227-6241, https://doi.org/10.5194/acp-17-
684   6227-2017, 2017.

685   Dai, L., Wang, H. L., Zhou, L. Y., An, J. L., Tang, L. L., Lu, C. S., Yan, W. L., Liu, R.
686   Y., Kong, S. F., Chen, M. D., Lee, S. H., and Yu, H.: Regional and local new
687   particle formation events observed in the Yangtze River Delta region, China, J
688   Geophys Res-Atmos, 122, 2389-2402, https://doi.org/10.1002/2016JD026030,
689   2017.

690   Dal Maso, M., Kulmala, M., Riipinen, I., Wagner, R., Hussein, T., Aalto, P. P., and
691   Lehtinen, K. E. J.: Formation and growth of fresh atmospheric aerosols: eight
692   years of aerosol size distribution data from SMEAR II, Hyytiala, Finland, Boreal
693   Environ Res, 10, 323-336, 2005.

de Jesus, A. L., Rahman, M. M., Mazaheri, M., Thompson, H., Knibbs, L. D., Jeong, C., Evans, G., Nei, W., Ding, A., Qiao, L., Li, L., Portin, H., Niemi, J. V., Timonen, H., Luoma, K., Petäjä, T., Kulmala, M., Kowalski, M., Peters, A., Cyrys, J., Ferrero, L., Manigrasso, M., Avino, P., Buonano, G., Reche, C., Querol, X., Beddows, D., Harrison, R. M., Sowlat, M. H., Sioutas, C., and Morawska, L.: Ultrafine particles and PM2.5 in the air of cities around the world: Are they representative of each other?, Environment International, 129, 118-135, 10.1016/j.envint.2019.05.021, 2019.

Du, W., Zhao, J., Wang, Y. Y., Zhang, Y. J., Wang, Q. Q., Xu, W. Q., Chen, C., Han, T. T., Zhang, F., Li, Z. Q., Fu, P. Q., Li, J., Wang, Z. F., and Sun, Y. L.: Simultaneous measurements of particle number size distributions at ground level and 260m on a meteorological tower in urban Beijing, China, Atmos Chem Phys, 17, 6797-6811, 2017.

Feng, X., Dang, Z., Huang, W., Shao, L., and Li, W.: Microscopic morphology and size distribution of particles in PM2.5 of Guangzhou City, Journal of Atmospheric Chemistry, 64, 37-51, http://doi.org/10.1007/s10874-010-9169-7, 2010.

Han, S. Q., Bian, H., Feng, Y. C., Liu, A. X., Li, X. J., Zeng, F., and Zhang, X. L.: Analysis of the Relationship between O3, NO and NO2 in Tianjin, China, Aerosol Air Qual Res, 11, 128-139, https://doi.org/10.4209/aaqr.2010.07.0055, 2011.

Hao, J. M., and Wang, L. T.: Improving urban air quality in China: Beijing case study, J Air Waste Manage, 55, 1298-1305, https://doi.org/10.1080/10473289.2005.10464726, 2005.

Hari, P., and Kulmala, M.: Station for measuring ecosystem-atmosphere relations (SMEAR II), Boreal Environ Res, 10, 315-322, 2005.

IPCC. IPCC, 2007: summary for policymakers. Climate change 2007, 93-129.

Jayaratne, R., Pushpawela, B., He, C. R., Li, H., Gao, J., Chai, F. H., and Morawska, L.: Observations of particles at their formation sizes in Beijing, China, Atmos Chem Phys, 17, 8825-8835, 2017.

Jiang, J. K., Zhao, J., Chen, M. D., Eisele, F. L., Scheckman, J., Williams, B. J., Kuang, C. A., and McMurry, P. H.: First Measurements of Neutral Atmospheric Cluster and 1-2 nm Particle Number Size Distributions During Nucleation Events, Aerosol Science and Technology, 45, Ii-V, https://dio.org/10.1080/02786826.2010.546817, 2011.

Kangasluoma, J., Franchin, A., Duplissy, J., Ahonen, L., Korhonen, F., Attoui, M., Mikkilä, J., Lehtipalo, K., Vanhanen, J., Kulmala, M., and Petäjä, T.: Operation of the Airmodus A11 nano Condensation Nucleus Counter at various inlet pressures and various operation temperatures, and design of a new inlet system, Atmos Meas Tech, 9, 2977-2988, https://doi.org/10.5194/amt-9-2977-2016, 2016.

Kerminen, V. M., Pirjola, L., and Kulmala, M.: How significantly does coagulational scavenging limit atmospheric particle production?, J Geophys Res-Atmos, 106, 24119-24125, https://doi.org/10.1029/2001jd000322, 2001.

Kerminen, V. M., Paramonov, M., Anttila, T., Riipinen, I., Fountoukis, C., Korhonen, H., Asmi, E., Laakso, L., Lihavainen, H., Swietlicki, E., Svenningsson, B., Asmi, A., Pandis, S. N., Kulmala, M., and Petäjä, T.: Cloud condensation nuclei

738   production associated with atmospheric nucleation: a synthesis based on existing
739   literature and new results, Atmos Chem Phys, 12, 12037-12059,
740   https://doi.org/10.5194/acp-12-12037-2012, 2012.

741 Kerminen, V. M., Chen, X. M., Vakkari, V., Petäjä, T., Kulmala, M., and Bianchi, F.:
742   Atmospheric new particle formation and growth: review of field observations,
743   Environ Res Lett, 13, https://doi.org/10.1088/1748-9326/aadf3c, 2018.

744 Kontkanen, J., Järvinen, E., Manninen, H. E., Lehtipalo, K., Kangasluoma, J., Decesari,
745   S., Gobbi, G. P., Laaksonen, A., Petäjä, T., and Kulmala, M.: High concentrations
746   of sub-3nm clusters and frequent new particle formation observed in the Po Valley,
747   Italy, during the PEGASOS 2012 campaign, Atmos Chem Phys, 16, 17,
748   https://doi.org/10.5194/acp-16-1919-2016, 2016.

749 Kontkanen, J., Lehtipalo, K., Ahonen, L., Kangasluoma, J., Manninen, H. E., Hakala,
750   J., Rose, C., Sellegri, K., Xiao, S., Wang, L., Qi, X. M., Nie, W., Ding, A. J., Yu,
751   H., Lee, S., Kerminen, V. M., Petaja, T., and Kulmala, M.: Measurements of sub-
752   3nm particles using a particle size magnifier in different environments: from
753   clean mountain top to polluted megacities, Atmos Chem Phys, 17, 2163-2187,
754   2017.

755 Koponen, I. K., Asmi, A., Keronen, P., Puhto, K., and Kulmala, M.: Indoor air
756   measurement campaign in Helsinki, Finland 1999 - the effect of outdoor air
757   pollution on indoor air, Atmospheric Environment, 35, 1465-1477,
758   https://doi.org/10.1016/s1352-2310(00)00338-1, 2001.

759 Kreyling, W. G., Semmler, M., and Möller, W.: Dosimetry and toxicology of ultrafine
760   particles, J Aerosol Med, 17, 140-152,
761   https://doi.org/10.1089/0894268041457147, 2004.

762 Kulmala, M.: How particles nucleate and grow, Science, 302, 1000-1001,
763   https://doi.org/10.1126/science.1090848, 2003.

764 Kulmala, M., Vehkamäki, H., Petäjä, T., Dal Maso, M., Lauri, A., Kerminen, V. M.,
765   Birmili, W., and McMurry, P. H.: Formation and growth rates of ultrafine
766   atmospheric particles: a review of observations, J Aerosol Sci, 35, 143-176,
767   https://doi.org/10.1016/j.jaerosci.2003.10.003, 2004.

768 Kulmala, M., Riipinen, I., Sipilä, M., Manninen, H. E., Petäjä, T., Junninen, H., Dal
769   Maso, M., Mordas, G., Mirme, A., Vana, M., Hirsikko, A., Laakso, L., Harrison,
770   R. M., Hanson, I., Leung, C., Lehtinen, K. E. J., and Kerminen, V. M.: Toward
771   direct measurement of atmospheric nucleation, Science, 318, 89-92,
772   https://doi.org/10.1126/science.1144124, 2007.

773 Kulmala, M., Petäjä, T., Nieminen, T., Sipilä, M., Manninen, H. E., Lehtipalo, K., Dal
774   Maso, M., Aalto, P. P., Junninen, H., Paasonen, P., Riipinen, I., Lehtinen, K. E. J.,
775   Laaksonen, A., and Kerminen, V. M.: Measurement of the nucleation of
776   atmospheric aerosol particles, Nat Protoc, 7, 1651-1667,
777   https://doi.org/10.1038/nprot.2012.091, 2012.

778 Kulmala, M., Kontkanen, J., Junninen, H., Lehtipalo, K., Manninen, H. E., Nieminen,
779   T., Petäjä, T., Sipilä, M., Schobesberger, S., Rantala, P., Franchin, A., Jokinen, T.,
780   Järvinen, E., Äijälä, M., Kangasluoma, J., Hakala, J., Aalto, P. P., Paasonen, P.,
781   Mikkilä, J., Vanhanen, J., Aalto, J., Hakola, H., Makkonen, U., Ruuskanen, T.,

Mauldin, R. L., Duplissy, J., Vehkamäki, H., Bäck, J., Kortelainen, A., Riipinen, I., Kurtén, T., Johnston, M. V., Smith, J. N., Ehn, M., Mentel, T. F., Lehtinen, K. E. J., Laaksonen, A., Kerminen, V. M., and Worsnop, D. R.: Direct Observations of Atmospheric Aerosol Nucleation, Science, 339, 943-946, https://doi.org/10.1126/science.1227385, 2013.

Kulmala, M., Petaja, T., Ehn, M., Thornton, J., Sipila, M., Worsnop, D. R., and Kerminen, V. M.: Chemistry of Atmospheric Nucleation: On the Recent Advances on Precursor Characterization and Atmospheric Cluster Composition in Connection with Atmospheric New Particle Formation, Annu Rev Phys Chem, 65, 21-37, 2014.

Kulmala, M.: Atmospheric chemistry: China's choking cocktail, Nature, 526, 497-499, https://doi.org/10.1038/526497a, 2015.

Kulmala, M., Kerminen, V. M., Petäjä, T., Ding, A. J., and Wang, L.: Atmospheric gas-to-particle conversion: why NPF events are observed in megacities?, Faraday Discuss, 200, 271-288, https://doi.org/10.1039/C6FD00257A, 2017.

Lehtipalo, K., Leppä, J., Kontkanen, J., Kangasluoma, J., Wimmer, D., Franchin, A., Schobesberger, S., Junninen, H., Petäjä, T., Sipilä, M., Mikkilä, J., Vanhanen, J., Worsnop, D. r., and Kulmala, M.: methods for determining particle size distribution and growth rates between 1 and 3 nm using the Particle Size Magnifier, Boreal Environ Res, 19, 215-236, 2014.

Lehtipalo, K., Yan, C., Dada, L., Bianchi, F., Xiao, M., Wagner, R., Stolzenburg, D., Ahonen, L. R., Amorim, A., Baccarini, A., Bauer, P. S., Baumgartner, B., Bergen, A., Bernhammer, A. K., Breitenlechner, M., Brilke, S., Buchholz, A., Mazon, S. B., Chen, D. X., Chen, X. M., Dias, A., Dommen, J., Draper, D. C., Duplissy, J., Ehn, M., Finkenzeller, H., Fischer, L., Frege, C., Fuchs, C., Garmash, O., Gordon, H., Hakala, J., He, X. C., Heikkinen, L., Heinritzi, M., Helm, J. C., Hofbauer, V., Hoyle, C. R., Jokinen, T., Kangasluoma, J., Kerminen, V. M., Kim, C., Kirkby, J., Kontkanen, J., Kurten, A., Lawler, M. J., Mai, H. J., Mathot, S., Mauldin, R. L., Molteni, U., Nichman, L., Nie, W., Nieminen, T., Ojdanic, A., Onnela, A., Passananti, M., Petäjä, T., Piel, F., Pospisilova, V., Quéléver, L. L. J., Rissanen, M. P., Rose, C., Sarnela, N., Schallhart, S., Schuchmann, S., Sengupta, K., Simon, M., Sipilä, M., Tauber, C., Tomé, A., Tröstl, J., Väisänen, O., Vogel, A. L., Volkamer, R., Wagner, A. C., Wang, M. Y., Weitz, L., Wimmer, D., Ye, P. L., Ylisirnio, A., Zha, Q. Z., Carslaw, K. S., Curtius, J., Donahue, N. M., Flagan, R. C., Hansel, A., Riipinen, I., Virtanen, A., Winkler, P. M., Baltensperger, U., Kulmala, M., and Worsnop, D. R.: Multicomponent new particle formation from sulfuric acid, ammonia, and biogenic vapors, Sci Adv, 4, https://doi.org/10.1126/sciadv.aau5363, 2018.

Lelieveld, J., Evans, J. S., Fnais, M., Giannadaki, D., and Pozzer, A.: The contribution of outdoor air pollution sources to premature mortality on a global scale, Nature, 525, 367-371, https://doi.org/10.1038/nature15371,2015.

Liu, X. G., Li, J., Qu, Y., Han, T., Hou, L., Gu, J., Chen, C., Yang, Y., Liu, X., Yang, T., Zhang, Y., Tian, H., and Hu, M.: Formation and evolution mechanism of regional

825 haze: a case study in the megacity Beijing, China, Atmos Chem Phys, 13, 4501-
826 4514, 2013.

827 Liu, J. Q., Jiang, J. K., Zhang, Q., Deng, J. G., and Hao, J. M.: A spectrometer for
828 measuring particle size distributions in the range of 3 nm to 10 mu m, Front Env
829 Sci Eng, 10, 63-72, https://doi.org/10.1007/s11783-014-0754-x,2016.

830 Lowry, D., Lanoiselle, M. E., Fisher, R. E., Martin, M., Fowler, C. M. R., France, J. L.,
831 Hernandez-Paniagua, I. Y., Novelli, P. C., Sriskantharajah, S., O'Brien, P., Rata,
832 N. D., Holmes, C. W., Fleming, Z. L., Clemitshaw, K. C., Zazzeri, G., Pommier,
833 M., McLinden, C. A., and Nisbet, E. G.: Marked long-term decline in ambient
834 CO mixing ratio in SE England, 1997-2014: evidence of policy success in
835 improving air quality, Sci Rep-Uk, 6, https://doi.org/10.1038/srep25661, 2016.

836 Lu, Y., Yan, C., Fu, Y., Chen, Y., Liu, Y., Yang, G., Wang, Y., Bianchi, F., Chu, B., Zhou,
837 Y., Yin, R., Baalbaki, R., Garmash, O., Deng, C., Wang, W., Liu, Y., Petäjä, T.,
838 Kerminen, V. M., Jiang, J., Kulmala, M., and Wang, L.: A proxy for atmospheric
839 daytime gaseous sulfuric acid concentration in urban Beijing, Atmos. Chem. Phys.
840 Discuss., 2018, 1-31, https://doi.org/10.5194/acp-2018-1132, 2018.

841 Lu, Z., Streets, D. G., Zhang, Q., Wang, S., Carmichael, G. R., Cheng, Y. F., Wei, C.,
842 Chin, M., Diehl, T., and Tan, Q.: Sulfur dioxide emissions in China and sulfur
843 trends in East Asia since 2000, Atmos Chem Phys, 10, 6311-6331,
844 https://doi.org/10.5194/acp-10-6311-2010, 2010.

845 Manninen, H. E., Mirme, S., Mirme, A., Petäjä, T., and Kulmala, M.: How to reliably
846 detect molecular clusters and nucleation mode particles with Neutral cluster and
847 Air Ion Spectrometer (NAIS), Atmos Meas Tech, 9, 3577-3605,
848 https://doi.org/10.5194/amt-9-3577-2016, 2016.

849 Mazon, S. B., Kontkanen, J., Manninen, H. E., Nieminen, T., Kerminen, V.-M., and
850 Kulmala, M.: A long-term comparison of nighttime cluster events and daytime
851 ion formation in a boreal forest, Boeral Environment Research, 21, 19, 2016.

852 Mirme, A., Tamm, E., Mordas, G., Vana, M., Uin, J., Mirme, S., Bernotas, T., Laakso,
853 L., Hirsikko, A., and Kulmala, M.: A wide-range multi-channel air ion
854 spectrometer, Boreal Environ Res, 12, 247-264, 2007.

855 Mirme, S., and Mirme, A.: The mathematical principles and design of the NAIS - a
856 spectrometer for the measurement of cluster ion and nanometer aerosol size
857 distributions, Atmos Meas Tech, 6, 1061-1071, https://doi.org/10.5194/amt-6-
858 1061-2013, 2013.

859 Oberdörster, G., Sharp, Z., Atudorei, V., Elder, A., Gelein, R., Kreyling, W., and Cox,
860 C.: Translocation of inhaled ultrafine particles to the brain, Inhal Toxicol, 16, 437-
861 445, https://doi.org/10.1080/08958370490439597, 2004.

862 Paasonen, P., Peltola, M., Kontkanen, J., Junninen, H., Kerminen, V.-M., and Kulmala,
863 M.: Comprehensive analysis of particle growth rates from nucleation mode to
864 cloud condensation nuclei in boreal forest, Atmos Chem Phys, 18, 12085-12103,
865 10.5194/acp-18-12085-2018, 2018.

866 Pétron, G., Granier, C., Khattatov, B., Yudin, V., Lamarque, J. F., Emmons, L., Gille, J.,
867 and Edwards, D. P.: Monthly CO surface sources inventory based on the 2000-

2001 MOPITT satellite data, Geophys Res Lett, 31, https://doi.org/10.1029/2004gl020560, 2004.

Pirjola, L., Lähde, T., Niemi, J. V., Kousa, A., Rönkkö, T., Karjalainen, P., Keskinen, J., Frey, A., and Hillamo, R.: Spatial and temporal characterization of traffic emissions in urban microenvironments with a mobile laboratory, Atmospheric Environment, 63, 156-167, https://doi.org/10.1016/j.atmosenv.2012.09.022, 2012.

Qi, X. M. D., A. J., Nie, W., Petaja, T., Kerminen, V. M., Herrmann, E., Xie, Y. N., Zheng, L. F., Manninen, H., Aalto, P., Sun, J. N., Xu, Z. N., Chi, X. G., Huang, X., Boy, M., Virkkula, A., Yang, X. Q., Fu, C. B., and Kulmala, M.: Aerosol size distribution and new particle formation in the western Yangtze River Delta of China: 2 years of measurements at the SORPES station, Atmos Chem Phys, 15, 12445-12464, 2015.

Ravishankara, A.R.: Heterogeneous and Multiphase Chemistry in the Troposphere, Science 276, 1058-1065, https://doi.org/ 10.1126/science.276.5315.1058,1997.

Roberts, D. L., and Jones, A.: Climate sensitivity to black carbon aerosol from fossil fuel combustion, J Geophys Res-Atmos, 109, https://doi.org/10.1029/2004jd004676, 2004.

Rönkkö, T., Kuuluvainen, H., Karjalainen, P., Keskinen, J., Hillamo, R., Niemi, J. V., Pirjola, L., Timonen, H. J., Saarikoski, S., Saukko, E., Järvinen, A., Silvennoinen, H., Rostedt, A., Olin, M., Yli-Ojanperä, J., Nousiainene, P., Kousa, A., and Dal Maso, M.: Traffic is a major source of atmospheric nanocluster aerosol, P Natl Acad Sci USA, 114, 7549-7554, https://doi.org/10.1073/pnas.1700830114, 2017.

Shi, J. P., and Harrison, R. M.: Investigation of Ultrafine Particle Formation during Diesel Exhaust Dilution, Environ. Sci. Technol., 33, 7, 1999.

Shi, J. P., Evans, D. E., Khan, A. A., and Harrison, R. M.: Sources and concentration of nanoparticles (< 10 nm diameter) in the urban atmosphere, Atmospheric Environment, 35, 1193-1202, 2001.

Solomos, S., Kallos, G., Kushta, J., Astitha, M., Tremback, C., Nenes, A., and Levin, Z.: An integrated modeling study on the effects of mineral dust and sea salt particles on clouds and precipitation, Atmos Chem Phys, 11, 873-892, https://doi.org/10.5194/acp-11-873-2011, 2011.

Tian, X., Xie, P. H., Xu, J., Li, A., Wang, Y., Qin, M., and Hu, Z. K.: Long-term observations of tropospheric NO2, SO2 and HCHO by MAX-DOAS in Yangtze River Delta area, China, J Environ Sci-China, 71, 207-221, https://doi.org/10.1016/j.jes.2018.03.006, 2018.

Vahlsing, C., and Smith, K. R.: Global review of national ambient air quality standards for PM10 and SO2 (24 h), Air Qual Atmos Hlth, 5, 393-399, https://doi.org/10.1007/s11869-010-0131-2, 2012.

Vanhanen, J., Mikkilä, J., Lehtipalo, K., Sipilä, M., Manninen, H. E., Siivola, E., Petäjä, T., and Kulmala, M.: Particle Size Magnifier for Nano-CN Detection, Aerosol Science and Technology, 45, 533-542, https://doi.org/10.1080/02786826.2010.547889, 2011.

von Bismarck-Osten, C., Birmili, W., Ketzel, M., Massling, A., Petäjä, T., and Weber, S.: Characterization of parameters influencing the spatio-temporal variability of urban particle number size distributions in four European cities, Atmospheric Environment, 77, 415-429, https://doi.org/10.1016/j.atmosenv.2013.05.029, 2013.

Vu, T. V., Delgado-Saborit, J. M., and Harrison, R. M.: Review: Particle number size distributions from seven major sources and implications for source apportionment studies, Atmospheric Environment, 122, 114-132, 10.1016/j.atmosenv.2015.09.027, 2015.

Wang, D. W., Guo, H., Cheung, K., and Gan, F. X.: Observation of nucleation mode particle burst and new particle formation events at an urban site in Hong Kong, Atmospheric Environment, 99, 196-205, https://doi.org/10.1016/j.atmosenv.2014.09.074, 2014a.

Wang, T., Xue, L. K., Brimblecombe, P., Lam, Y. F., Li, L., and Zhang, L.: Ozone pollution in China: A review of concentrations, meteorological influences, chemical precursors, and effects, Science of the Total Environment, 575, 1582-1596, https://doi.org/10.1016/j.scitotenv.2016.10.081, 2017.

Wang, Y. S., Yao, L., Wang, L. L., Liu, Z. R., Ji, D. S., Tang, G. Q., Zhang, J. K., Sun, Y., Hu, B., and Xin, J. Y.: Mechanism for the formation of the January 2013 heavy haze pollution episode over central and eastern China, Sci China Earth Sci, 57, 14-25, https://doi.org/10.1007/s11430-013-4773-4, 2014b.

Wang, Z. B., Hu, M., Wu, Z. J., Yue, D. L., He, L. Y., Huang, X. F., Liu, X. G., and Wiedensohler, A.: Long-term measurements of particle number size distributions and the relationships with air mass history and source apportionment in the summer of Beijing, Atmos Chem Phys, 13, 10159-10170, https://doi.org/10.5194/acp-13-10159-2013, 2013.

Wehner, B., Wiedensohler, A., Tuch, T. M., Wu, Z. J., Hu, M., Slanina, J., and Kiang, C. S.: Variability of the aerosol number size distribution in Beijing, China: New particle formation, dust storms, and high continental background, Geophys Res Lett, 31, https://doi.org/10.1029/2004GL021596, 2004.

WHO. Health and health behaviour among young people: health behaviour in school-aged children: a WHO cross-national study (HBSC), international report; WHO: 2000.

Wu, Z. J., Hu, M., Liu, S., Wehner, B., Bauer, S., Ssling, A. M., Wiedensohler, A., Petaja, T., Dal Maso, M., and Kulmala, M.: New particle formation in Beijing, China: Statistical analysis of a 1-year data set, J Geophys Res-Atmos, 112, 2007.

Wu, Z. J., Hu, M., Lin, P., Liu, S., Wehner, B., and Wiedensohler, A.: Particle number size distribution in the urban atmosphere of Beijing, China, Atmospheric Environment, 42, 7967-7980, https://doi.org/10.1016/j.atmosenv.2008.06.022, 2008.

Xiao, S., Wang, M. Y., Yao, L., Kulmala, M., Zhou, B., Yang, X., Chen, J. M., Wang, D. F., Fu, Q. Y., Worsnop, D. R., and Wang, L.: Strong atmospheric new particle formation in winter in urban Shanghai, China, Atmos Chem Phys, 15, 1769-1781, https://doi.org/10.5194/acp-15-1769-2015, 2015.

Yang, M., Ma, T. M., and Sun, C. W.: Evaluating the impact of urban traffic investment on SO2 emissions in China cities, Energ Policy, 113, 20-27, https://doi.org/10.1016/j.enpol.2017.10.039, 2018.

Yao, L., Garmash, O., Bianchi, F., Zheng, J., Yan, C., Kontkanen, J., Junninen, H., Mazon, S. B., Ehn, M., Paasonen, P., Sipilä, M., Wang, M. Y., Wang, X. K., Xiao, S., Chen, H. F., Lu, Y. Q., Zhang, B. W., Wang, D. F., Fu, Q. Y., Geng, F. H., Li, L., Wang, H. L., Qiao, L. P., Yang, X., Chen, J. M., Kerminen, V. M., Petäjä, T., Worsnop, D. R., Kulmala, M., and Wang, L.: Atmospheric new particle formation from sulfuric acid and amines in a Chinese megacity, Science, 361, 278-281, https://doi.org/10.1126/science.aao4839, 2018.

Yu, H., Zhou, L. Y., Dai, L., Shen, W. C., Dai, W., Zheng, J., Ma, Y., and Chen, M. D.: Nucleation and growth of sub-3nm particles in the polluted urban atmosphere of a megacity in China, Atmos Chem Phys, 16, 2641-2657, http://doi.org/10.5194/acp-16-2641-2016, 2016.

Yue, D. L., Hu, M., Wu, Z. J., Guo, S., Wen, M. T., Nowak, A., Wehner, B., Wiedensohler, A., Takegawa, N., Kondo, Y., Wang, X. S., Li, Y. P., Zeng, L. M., and Zhang, Y. H.: Variation of particle number size distributions and chemical compositions at the urban and downwind regional sites in the Pearl River Delta during summertime pollution episodes, Atmos Chem Phys, 10, 9431-9439, https://doi.org/10.5194/acp-10-9431-2010, 2010.

Zheng, G. J., Duan, F. K., Su, H., Ma, Y. L., Cheng, Y., Zheng, B., Zhang, Q., Huang, T., Kimoto, T., Chang, D., Pöschl, U., Cheng, Y. F., and He, K. B.: Exploring the severe winter haze in Beijing: the impact of synoptic weather, regional transport and heterogeneous reactions, Atmos Chem Phys, 15, 2969-2983, https://doi.org/10.5194/acp-15-2969-2015, 2015.

984   Tables and Figures

985   Table 1. Calendar of different types of days during our observations. NPF event days
986   are marked in green and haze days are marked in grey, whereas missing or undefined
987   days are marked in white.

988

989

990 Table 2a: Correlation coefficients between size segregated particle number
991 concentrations and trace gases mixing ratios/ PM$_{2.5}$ concentration on the NPF event
992 days. The time window was 08:00 - 14:00. High correlation coefficients (|R|>0.5) are
993 marked with bold and italic.

	CO	SO$_2$	NO$_x$	O$_3$	PM$_{2.5}$
Cluster	-0.61[a]	-0.16[a]	***-0.66***[a]	0.16[a]	***-0.66***[c]
Nucleation	-0.5[b]	-0.17[b]	***-0.55***[b]	0.36[b]	***-0.54***[c]
Aitken	***0.58***[b]	***0.55***[b]	***0.66***[b]	0.32[b]	0.33[c]
Accumulation	***0.71***[b]	***0.65***[b]	***0.69***[b]	0.15[b]	***0.83***[c]

994 [a] included 665 data points (the time resolution was 12 minutes), [b] included 1620 data
995 points (the time resolution was 5 min), [c] included 151 data points (the time resolution
996 was 1 hour).

997

998 Table 2b: Correlation coefficients between size segregated particle number
999 concentrations and trace gases mixing ratios/ PM$_{2.5}$ concentration on haze days. The
1000 time window was 08:00 - 14:00. High correlation coefficients (|R|>0.5) are marked
1001 with bold and italic.

	CO	SO$_2$	NO$_x$	O$_3$	PM$_{2.5}$
Cluster	-0.19[a]	0.09[a]	0.02[a]	0.13[a]	0.01[c]
Nucleation	-0.24[b]	0.07[b]	0.31[b]	0.17[b]	-0.33[c]
Aitken	0.10[b]	0.03[b]	0.44[b]	0.41[b]	-0.5[c]
Accumulation	***0.71***[b]	***0.76***[b]	0.37[b]	0.17[b]	***0.81***[c]

1002 [a] included 620 data points (the time resolution was 12 minutes), [b] included 1460 data
1003 points (the time resolution was 5 min), [c] included 89 data points (the time resolution
1004 was 1 hour).

1005

1006

1007 Table 3a: Correlation coefficients between particle number concentration of every
1008 mode on NPF event days. The time window was 08:00 - 14:00. High correlation
1009 coefficients (|R|>0.5) are marked with bold and italic.

	Cluster	Nucleation	Aitken	Accumulation
Cluster	1			
Nucleation	0.76 [a]	1		
Aitken	-0.46 [a]	-0.33 [b]	1	
Accumulation	-0.66 [a]	-0.66 [c]	0.7 [c]	1

1010 [a] included 516 data points (the time resolution was 12 minutes), [b] included 1251 data
1011 points (the time resolution was 5 min), [c] included 1331 data points (the time
1012 resolution was 5 min).

1013

1014 Table 3b: Correlation coefficients between particle number concentration of every
1015 mode on haze days. The time window was 08:00 - 14:00. High correlation
1016 coefficients (|R|>0.5) are marked with bold and italic.

	Cluster	Nucleation	Aitken	Accumulation
Cluster	1			
Nucleation	0.74 [a]	1		
Aitken	0.41 [a]	0.48 [b]	1	
Accumulation	-0.22 [a]	-0.33 [c]	-0.5 [c]	1

1017 [a] included 342 data points (the time resolution was 12 minutes), [b] included 824 data
1018 points (the time resolution was 5 min), [c] included 845 data points (the time resolution
1019 was 5 min).

1020
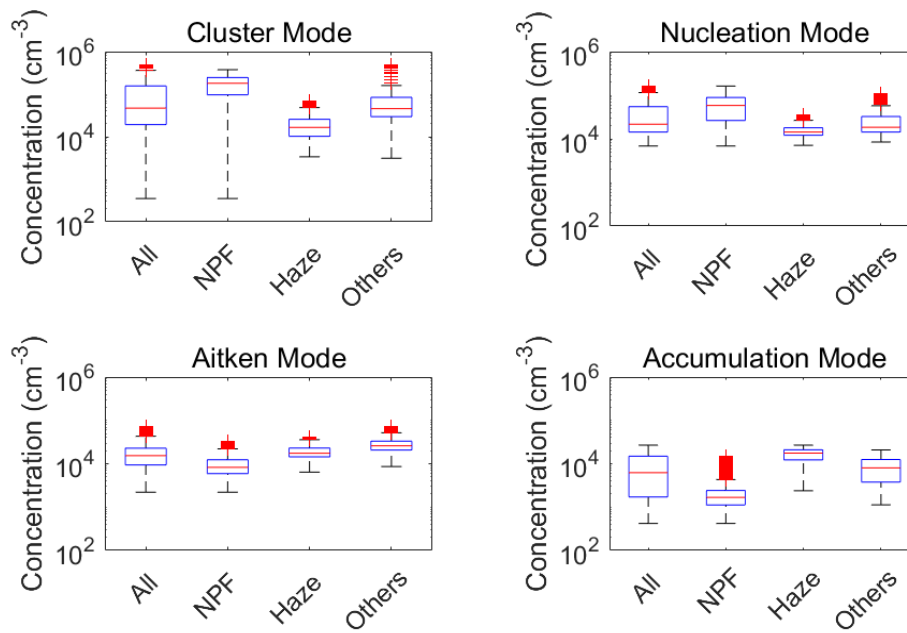
1021

Figure 1. Particle number concentrations in the cluster, nucleation, Aitken and accumulation mode on all the days, NPF event days, haze days and other days. The whiskers include 99.3% of data of every group. Data out of 1.5 × interquartile range are posited outside the whiskers and considered as outliers. The lines in the boxes represent the median value, the lower of the boxes represent 25% of the particle number concentration and the upper of the boxes represent 75% of the particle number concentration. Data marked with red pluses represent outliers.

1029
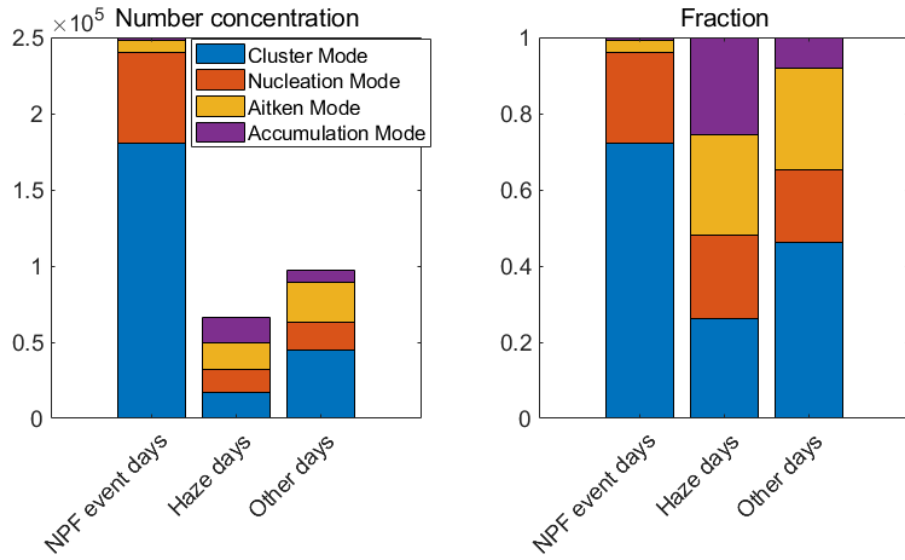
Figure 2. The median size-segregated number concentrations (left) and the median fraction of each mode to the total particle number concentration (right) on the NPF event days, haze days and other days.
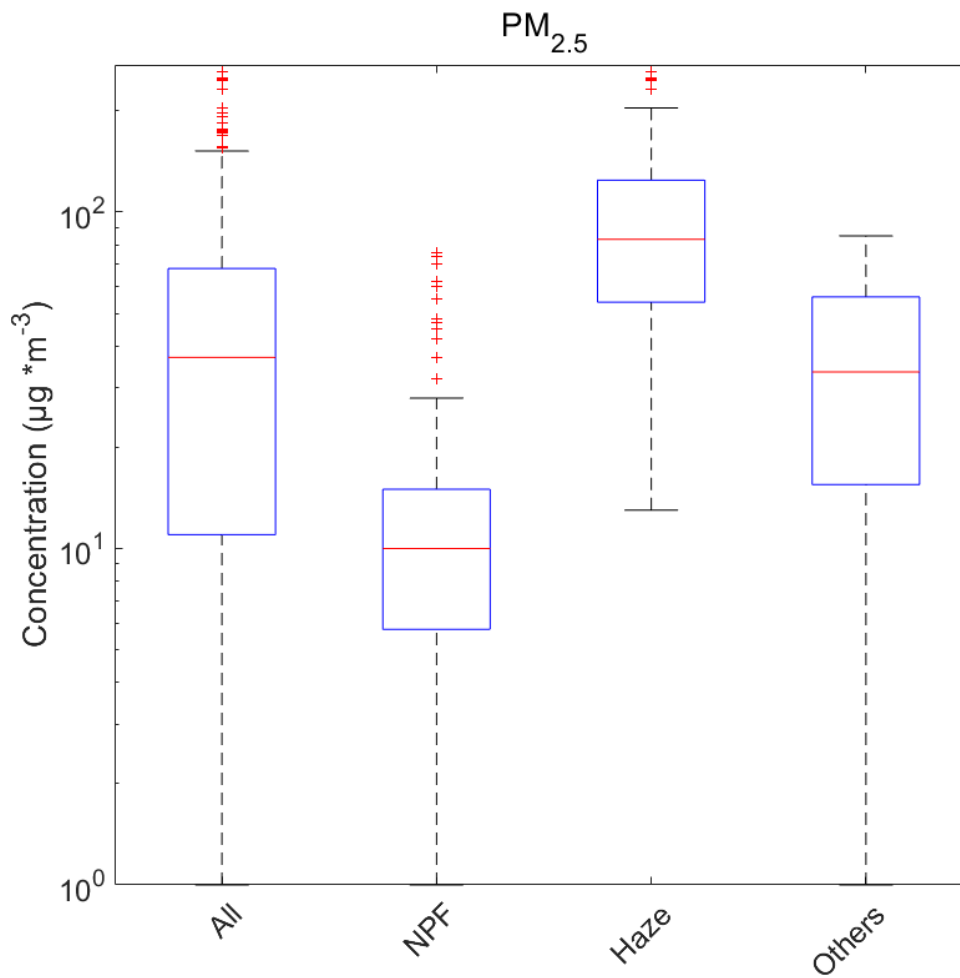
PM$_{2.5}$

1035

Figure 3. General character of the PM$_{2.5}$ mass concentration on all the days, NPF event days, haze days, and others days. The boxes show the median (red line) and 25% and 75% percentiles of the PM$_{2.5}$ mass concentration. Data marked with red pluses represent outliers as in Figure 1.

1040
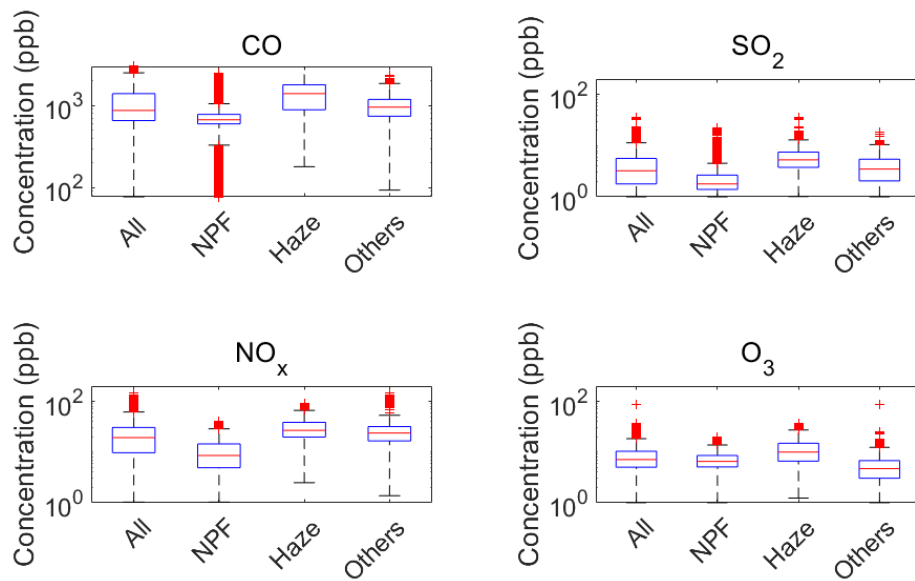
1041

1042 Figure 4. Trace gases mixing ratios of CO, SO_2, NO_x and O_3 on all the days, NPF event
1043 days, haze days and other days. The boxes show the median (red line) and 25% and 75%
1044 percentiles of the mixing ratios. Data marked with red pluses represent outliers as in
1045 Figure 1.

1046

1047
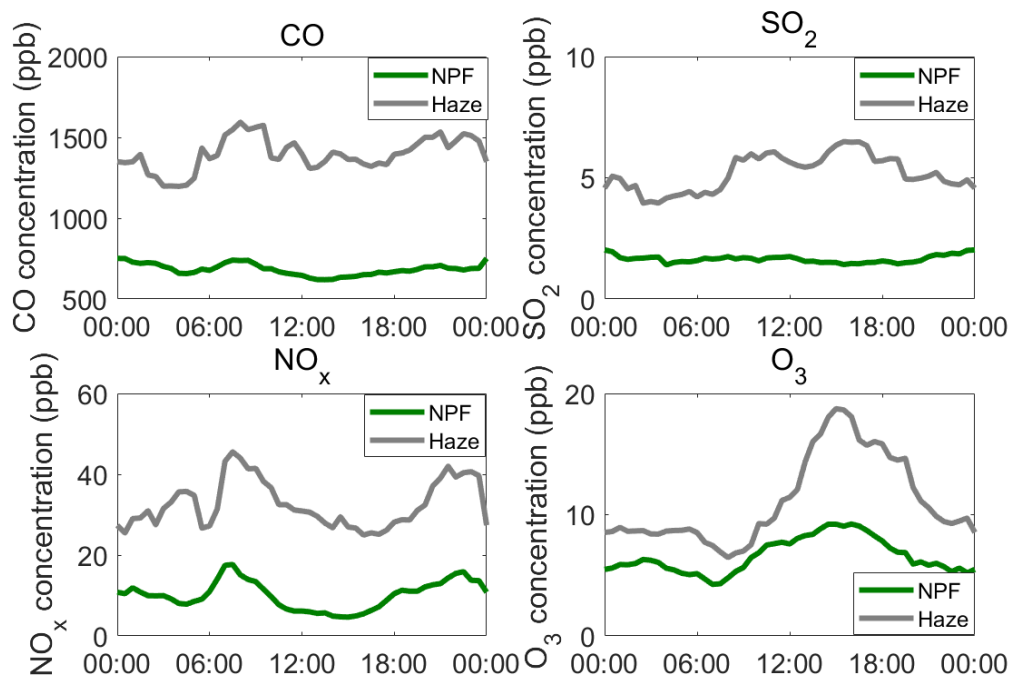
1048

Figure 5. Diurnal variation of trace gas (CO, SO$_2$, NO$_x$ and O$_3$ separately) mixing ratios on the NPF event days (green lines) and haze days (grey lines) separately. The time resolution was 30 minutes for every data point. Every data point here represents the median of all data at the same time of the days.

1053

1054
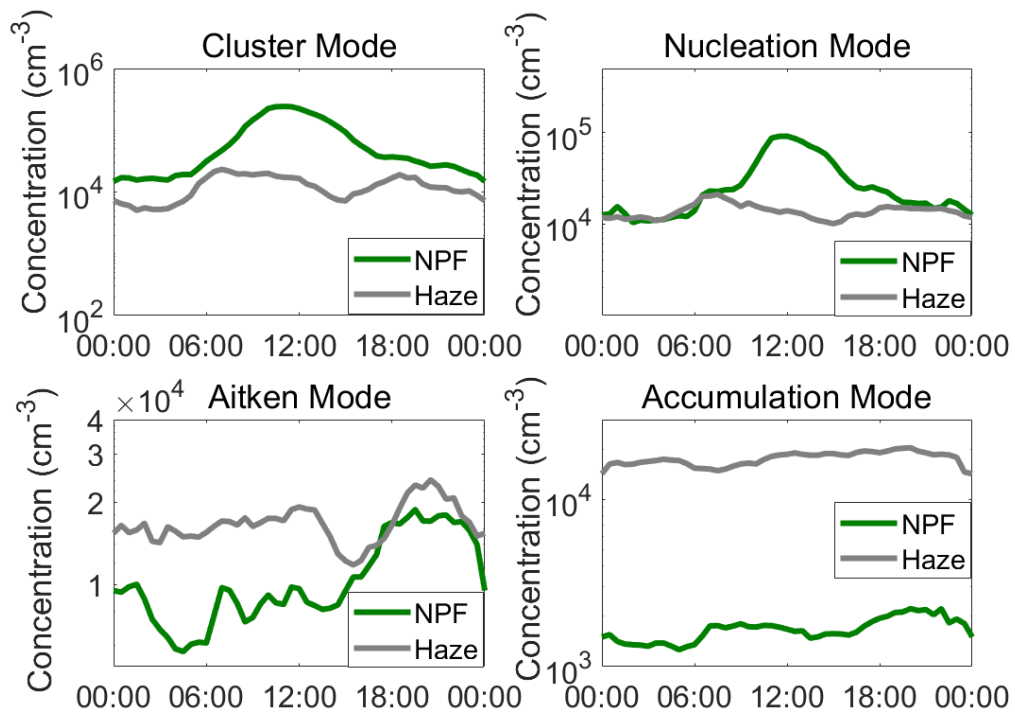
1055

1056 Figure 6. Diurnal variation of particle number concentration of every mode (cluster,
1057 nucleation, Aitken and accumulation mode separately) on the NPF event days (green
1058 lines) and haze days (grey lines). The time resolution was 30 min for every data point.
1059 Every data point here represents the median of all data at the same time of the days.
1060
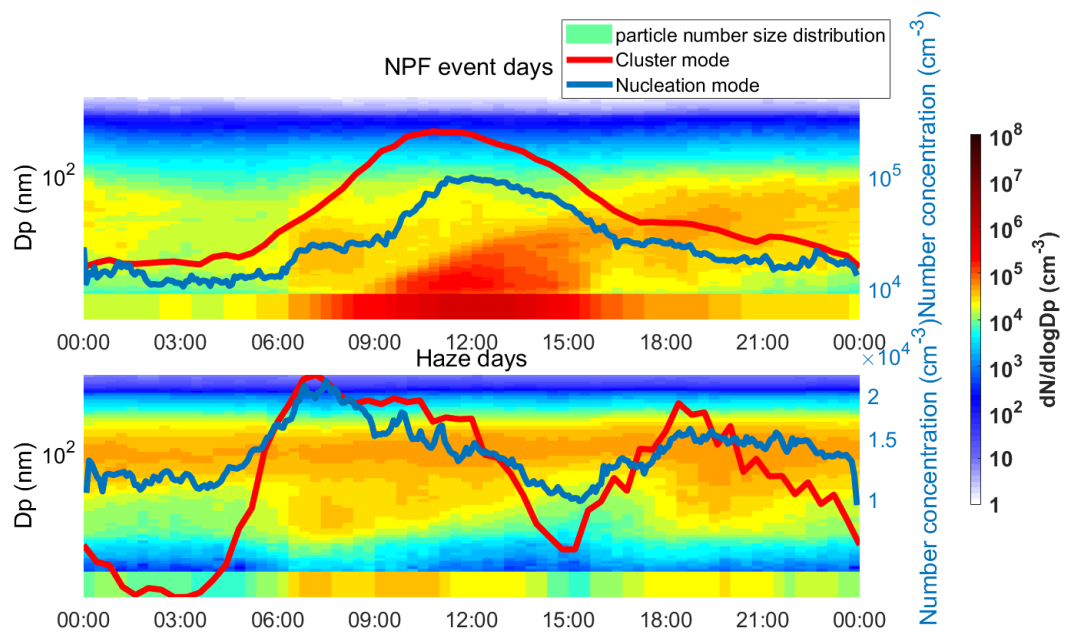
Figure 7. Median diurnal patterns of the particle number size distribution over the size range of 1.5-1000 nm and number concentrations of cluster mode (red lines) and nucleation mode (blue lines) particles on the NPF event days (upper panel) and haze days (lower panel). The time resolution for every data point of particle number size distribution and cluster mode particle number concentration was 12 minutes. The time resolution of every data point of nucleation mode particle number concentration was 5 minutes.

1071
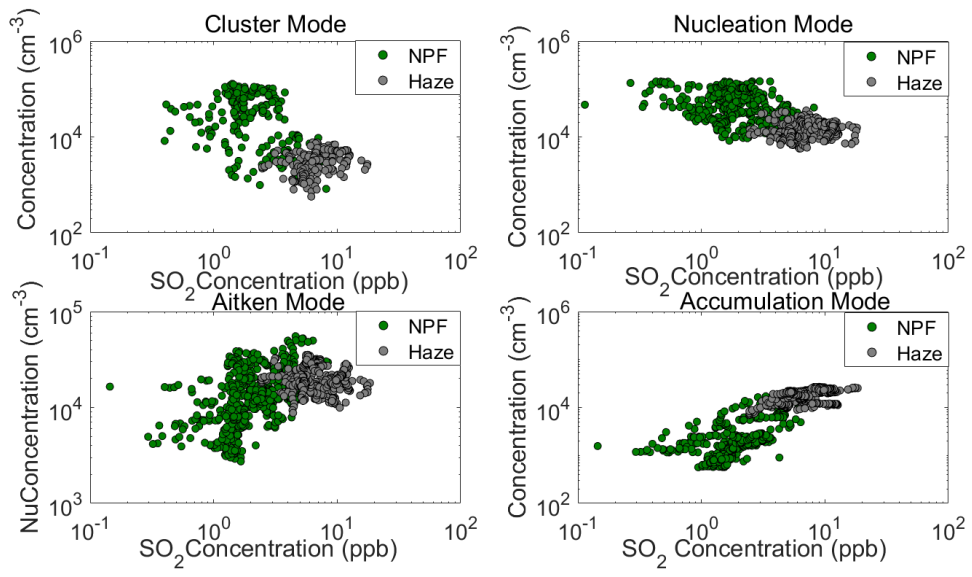
1072

1073 Figure 8. Relation between the SO_2 concentration and particle number concentration in
1074 each mode. The time resolution of the data points was 1 hour.

1075

1076
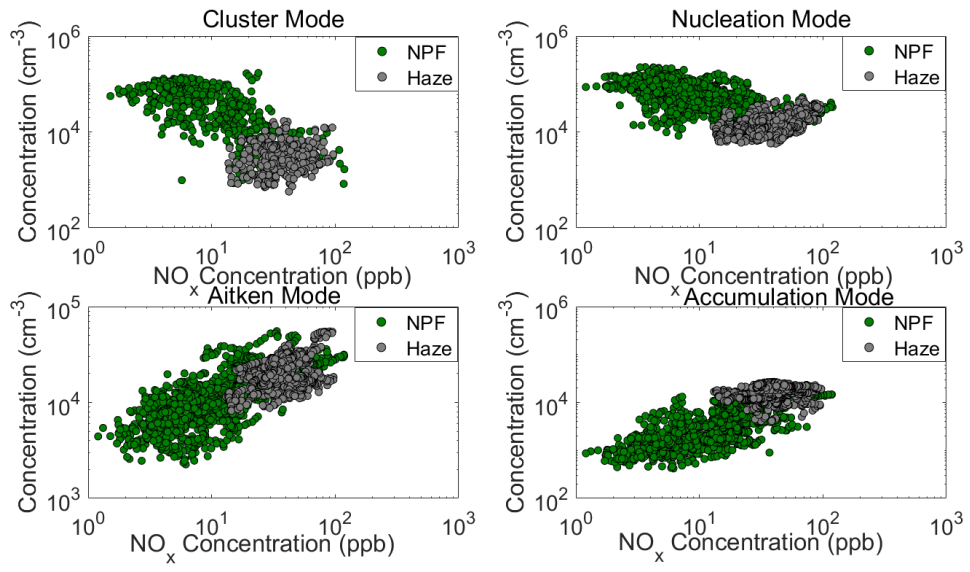
1077

1078 Figure 9. Relation between the NO_x concentration and particle number concentration
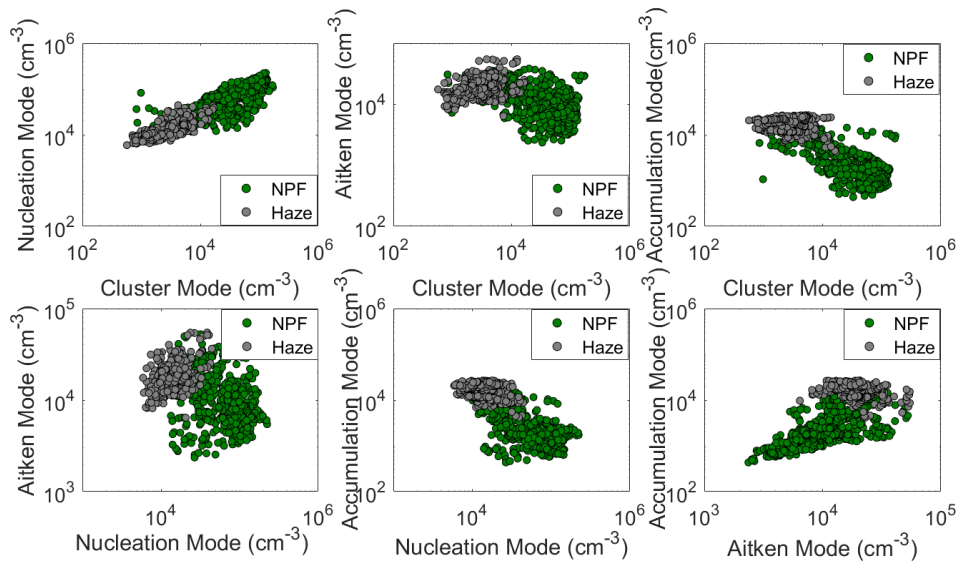1079 in each mode. The time resolution of the data points was 1 hour.

1080
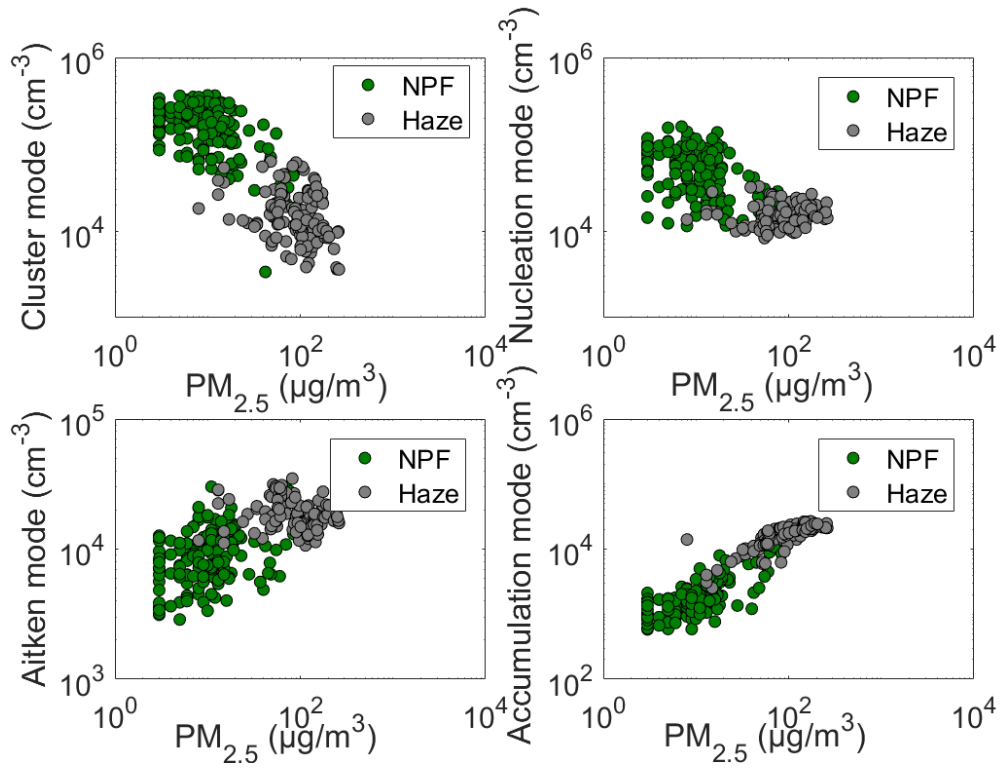
1081

Figure 10. Correlation between $PM_{2.5}$ concentration and particle number concentration in each mode on the NPF event days (green dots) and haze days (grey dots) separately. The time resolution of the data points was 1 hour.

1085

1086

1087

Figure 11. Correlation between every mode each other on NPF event days (green
dots) and haze days (grey dots). The time resolution of data in the plots of correlation
between cluster mode and other modes was 12 min and the time resolution of other
data points was 5 min.

1093
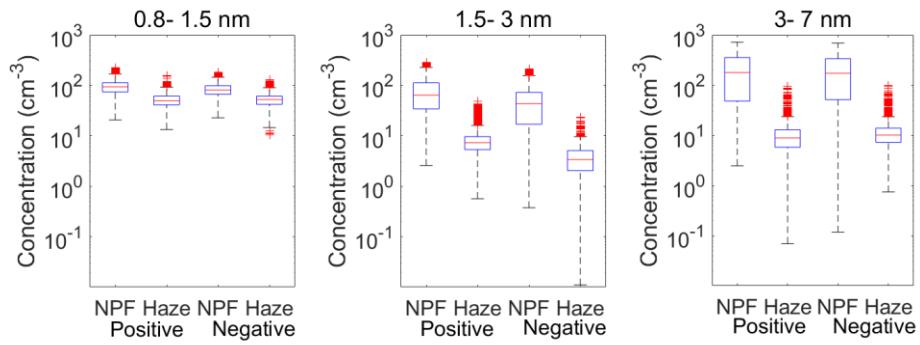
Figure 12. Positive and negative ion number concentrations in the size bins of 0.8-1.5nm, 1.5-3 nm and 3-7 nm on NPF event days and haze days separately. The whiskers include 99.3% of data of every group. Data out of 1.5 × interquartile range are posited outside the whiskers and considered as outliers. The lines in the boxes represent the median value, the lower of the boxes represent 25% of the number concentration, and the upper of the boxes represent 75% of the number concentration. Data marked with red pluses represent outliers.

1101
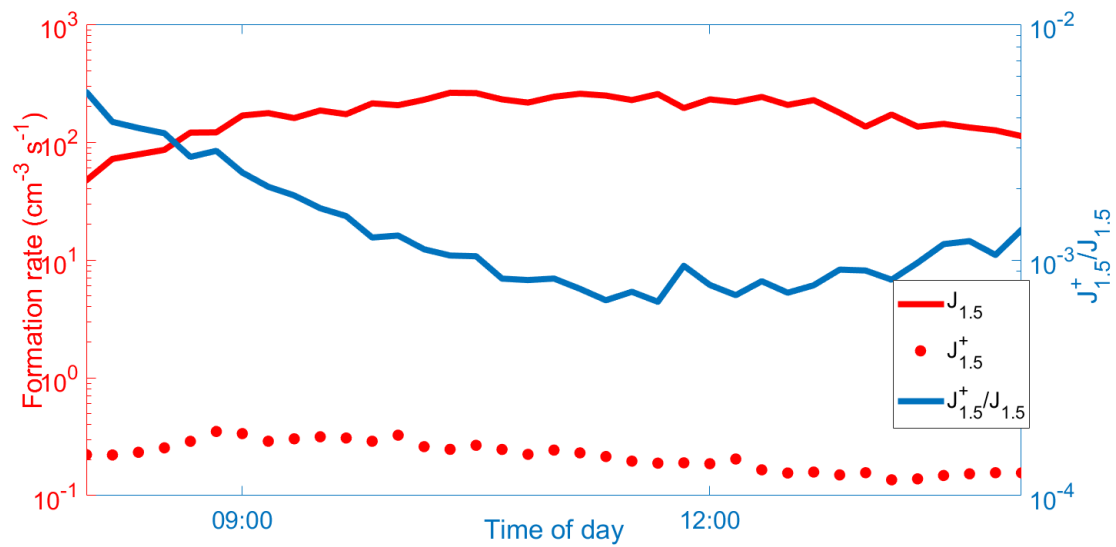
1102
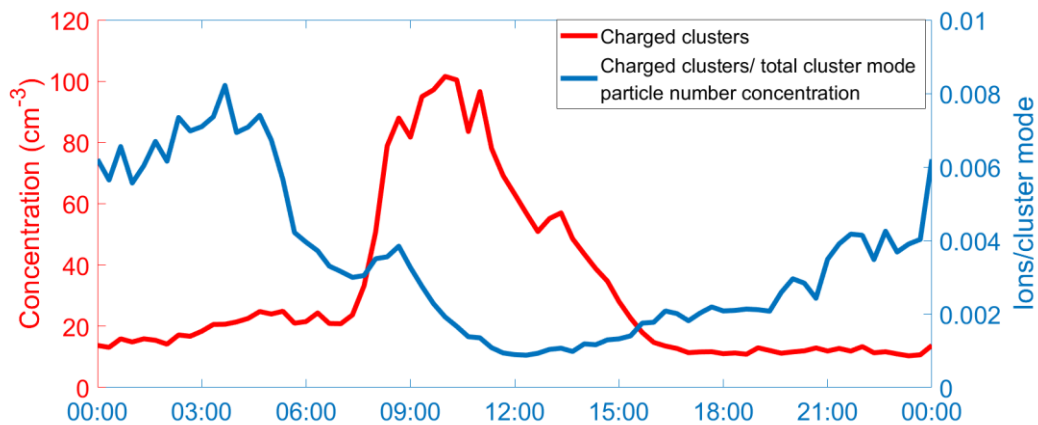
1103

Figure 13. Diurnal pattern of charged clusters (1.5-3 nm) number concentration (red line) and ratio of charged clusters to total cluster mode (1.5-3 nm) particle number concentration on the NPF event days (blue line). The time resolution of the used data was 12 min.
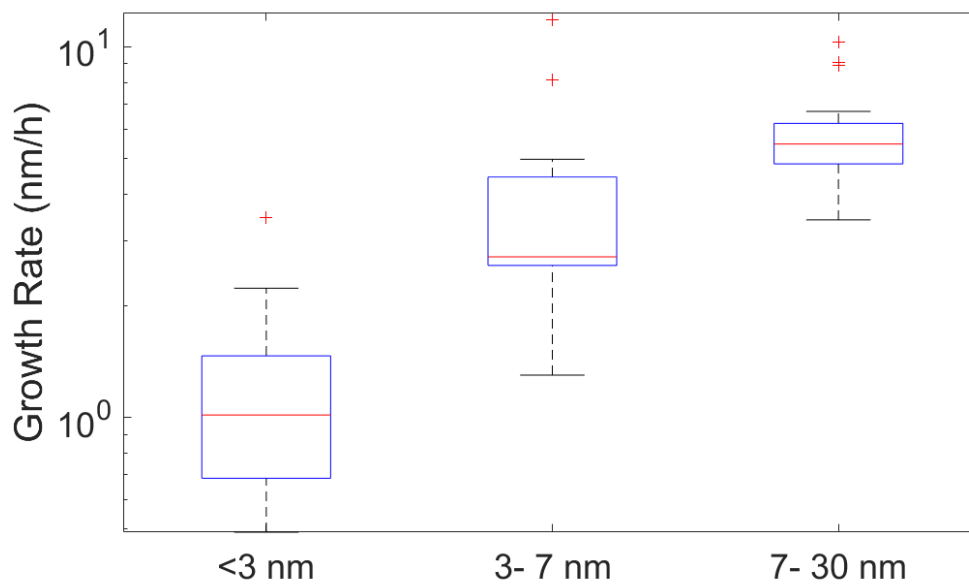
1110

Figure 14. Diurnal pattern of formation rate of positive charged clusters of 1.5 nm (red dots) and neutral clusters of 1.5 nm (red line) and the ratio between them (blue line) on the NPF event days during the NPF time window we chose. The time resolution of the used data was 12 min.

1111
1112
1113
1114

1115

1116

Figure 15. Growth rates of cluster mode and nucleation mode particles generated from NPF events. The lines in the boxes represent the median value, the lower of the boxes represent 25% of the growth rates and the upper of the boxes represent 75% of the growth rates. Data marked with red pluses represent outliers.